Univerzita Karlova v Praze

Matematicko-fyzikální fakulta

BAKALÁŘSKÁ PRÁCE

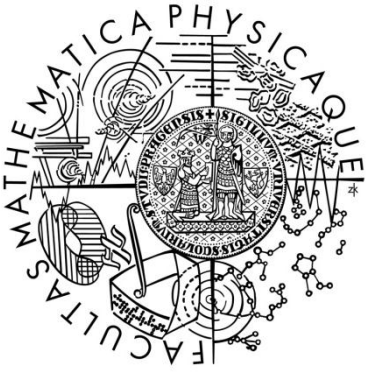

Tadeáš Bilka

Vývoj křemíkového detektoru pro experiment Belle II

Ústav částicové a jaderné fyziky

Vedoucí bakalářské práce: RNDr. Peter Kodyš, CSc.

Studijní program: Fyzika

Studijní obor: Obecná fyzika

Praha 2012

Charles University in Prague

Faculty of Mathematics and Physics

BACHELOR THESIS

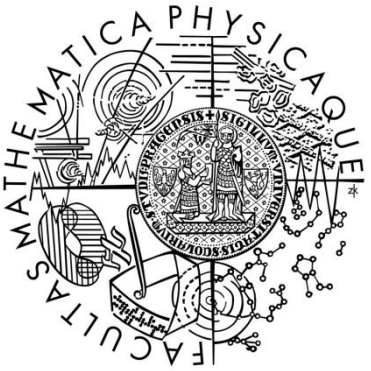

Tadeáš Bilka

Development of semiconductor detector for the Belle II experiment

Institute of Particle and Nuclear Physics

Supervisor of the bachelor thesis: Peter Kodyš, PhD.

Study Programme: Physics

Specialization: General Physics

Prague 2012

I would like to thank my supervisor, Peter Kodyš for his assistance and inspiring ideas, and Peter Kvasnička for his help in understanding the techniques used in high energy physics. Finally I would to thank to my father for his support, without which my studies would be hardly imaginable.

I declare that I carried out this bachelor thesis independently, and only with the cited sources, literature and other professional sources.

I understand that my work relates to the rights and obligations under the Act No. 121/2000 Coll., the Copyright Act, as amended, in particular the fact that the Charles University in Prague has the right to conclude a license agreement on the use of this work as a school work pursuant to Section 60 paragraph 1 of the Copyright Act.

Prague, May 23, 2012

Název práce: Vývoj křemíkového detektoru pro experiment Belle II

Autor: Tadeáš Bilka

Katedra / Ústav: Ústav částicové a jaderné fyziky

Vedoucí bakalářské práce: RNDr. Peter Kodyš CSc., Ústav částicové a jaderné fyziky

Abstrakt: Předložená bakalářská práce popisuje simulaci pixelového křemíkového detektoru DEPFET. Detektor DEPFET je klíčovou součástí nově budovaného detektoru částic Belle II v Japonském KEKu. Simulace je vytvořena jako balíček frameworku basf2, který je pro experiment Belle II vyvíjen. Cílem práce bylo seznámení se s experimentem Belle II, pixelovými detektory DEPFET a prostředím basf2 a vytvoření simulačního prostředí, které zachycuje experimentální uspořádání z roku 2009 v CERNu na urychlovači SPS. V úvodní části práce je popsán detektor Belle II, prostředí basf2 a jsou shrnuty základní informace o křemíkových detektorech, zejména o technologii DEPFET, následuje popis geometrie a samotné simulace. Úkolem analýzy je vyhodnocení odchylek (tzv. residuálů) změřených poloh od fitovaných drah částic a informací z clusterů v pixelovém detektoru. Závěrem je software použit pro simulaci ztenčovaného detektoru DEPFET vyvíjeného pro experiment Belle II.

Klíčová slova: beam test, simulace, pixelový detektor, polovodičový detektor, DEPFET, basf2, Belle II

Title: Development of semiconductor detector for the Belle II experiment

Author: Tadeáš Bilka

Department: Institute of Particle and Nuclear Physics

Supervisor: Peter Kodyš PhD., Institute of Particle and Nuclear Physics

Abstract: This bachelor thesis describes a simulation of the DEPFET pixel semiconductor detector. The DEPFET detector is a key part of a newly constructed Belle II particle detector being built in KEK, Japan. The simulation is made as a package for the basf2 framework, developed for the Belle II experiment. The goal of this thesis was to learn about the Belle II experiment, DEPFET pixel detector and the basf2 framework and to develop a simulation environment, depicting experimental setup at CERN's SPS accelerator in 2009. First part of this thesis describes the Belle II detector, the basf2 framework and summarizes basic information about silicon particle detectors, especially about the DEPFET technology. A task for the analysis of the data is to evaluate residuals after particle track fitting and cluster information in the pixel detector. Finally the simulation with thinned DEPFET sensor being developed for the Belle II is done.

Keywords: beam test, simulation, pixel detector, semiconductor detector, DEPFET, basf2, Belle II

Contents

Introduction

Particle physics has brought a significant progress in understanding laws of nature in past decades. However, many answered questions have been replaced by new problems. One example is the *CP* violation, which addresses differences between matter and antimatter behaviour under charge and parity conjugation[1]. Although this asymmetry is essential to explain matter predominance in our universe, observed interactions in experiments conducted so far are not enough to explain this obvious observation. One of the experiments related to *CP* violation was the Belle at KEKB accelerator. Its ancestor, the Belle II experiment is going to continue in investigation of this phenomenon.

Generally, particle physics experiments require substantial resources, human and financial. Thus large international collaborations are formed and any intended experiment has to be conscientiously prepared prior to its construction. Validation of the experiment and its ability to reach expected physical performance is typically checked using computer simulations and experimental testing of individual sub-components of the experiment. Tools for such simulations have been intensively developed for recent experiments and have been thoroughly cross-checked by their results.

Pixel silicon detectors are commonly used in particle detectors for precise spatial reconstruction. Thanks high level of integration, very tiny semiconductor devices can be manufactured. High granularity of the pixel detectors allows very precise position measurements, but limits the signal in individual pixels produced by charged particles. This issue is solved in the DEPFET technology by internal signal amplification in every single pixel.

The DEPFET detectors are planned to be an ingredient part of the Belle II particle detector (see next chapter). Development of these detectors includes modelling of their response in simulations and verification in experiments. The DEPFET detectors are regularly tested in real conditions at particle accelerators in so called **beam tests**. Beam tests allow understanding DEPFET properties in high energy conditions and to analyse detectors' spatial resolutions, select best readout

[1] The symmetry that holds generally is CPT (charge & parity & time inverse) conjugation. [4]

methods, operation voltages and other parameters, evaluate response of irradiated sensors and train the personnel. Such a beam test, conducted at CERN in 2009, is a model for computer simulation, whose development and results are presented in this work.

In this bachelor thesis, development of the beam test geometry setup, simulation and analysis is described and analysis results are presented. The software is made as a package for the basf2 framework, which has been developed for the Belle II experiment. It uses as much from the framework as possible, and offers an illustrative example of framework usage and related development. The behaviour of the digitizer and clusterizer (still under development) modules can be studied, in addition. Finally, because a set of experimental data from the 2009 beam test is available, the whole framework simulation and DEPFET digitization can be validated against real experimental results.

First part of the thesis offers an introduction to the Belle II experiment and mainly focuses on the detector itself. In section 2.2, the DEPFET technology is described. A brief overview of the basf2 framework is given in section 3.

The ground of the work done is in the development of the simulation and analysis software in basf2 environment and further analysis in ROOT. Section 4 presents the basic geometry setup and its software implementation. Simulation of particle passage through the detectors and DEPFET digitization rely on modules available in the framework; their basic functionality is explained in section 5. Overview of the newly developed analysis module is given in section 6.

Developed analysis software allows us to study different simulation scenarios. Analysis results are presented in section 7 and discussed in section 8. This thesis is mainly concerned in simulating DEPFET matrices from the 2009 beam test. Additionally, it shows results of thinned matrices planned for the Belle II detector.

The source code with basic examples is included on the attached CD-ROM. See the attachments section for information on how to use the software and where to find the source code online.

1. Belle II Experiment

1.1 Breaking Symmetry at KEK

Since 1999, when the Belle experiment has begun its operation, an exciting exploration into mysteries of the standard model (SM) and new physics scenarios behind has been established. The Belle was an experiment installed on the KEKB accelerator at High Energy Accelerator Research Company (KEK) in Tsukuba, Japan. The Belle had been operating until 2010 and its total integrated luminosity had exceeded 1ab^{-1}. KEKB accelerator holds the record of both highest instantaneous and integrated luminosity and the Belle experiment achieved unprecedented scientific results, which led to the 2008 Nobel Prize in Physics for Makoto Kobayashi and Toshihide Maskawa "for the discovery of the origin of the broken symmetry which predicts the existence of at least three families of quarks in nature" [1].

The main goal of the Belle was to learn about the *CP* violation through precise measurements of $\Upsilon(4S)$[2] decay channels created in collisions of asymmetric electron and positron beams. Centre of mass of the collision is tuned to rest energy of the resonance. The $\Upsilon(4S)$ resonance rest mass is just above a threshold for $B\bar{B}$ production, which explains why we talk about *B*-Factories. Many discoveries had been achieved at the Belle. It contributed to the discovery of *CP* violation in neutral B meson systems, where several decay channels were studied and mixing-induced time-dependent *CP* violation was observed. Measurements of the CKM matrix elements (CKM stands for Cabibbo–Kobayashi–Maskawa matrix) and related quantities, especially its complex phase related to the CKM unitarity triangle, were performed. New charmonia like resonance *X*(3872) was discovered and thoroughly studied. With the BaBar, discovery of mixing in systems of neutral charmed mesons D^0 was announced. There are many more examples, of which some point to some discrepancies between the experiment and SM predictions. An insight into new physics, behind the SM, would be possible with much larger data sample achieved by

[2] Several excited states of the Υ resonance (a meson consisting of bottom quark and antiquark) have been studied. Biggest data sample has been taken for the Υ (4S) resonance with rest mass 10.5794±0.0012 GeV/c^2 [3].

upgrading the KEKB accelerator to the SuperKEKB and introducing the new Bell II detector. [2], [3], [4]

1.2 Towards Belle II

To further investigate observed phenomena and provide a deeper insight into physics behind the SM, an upgrade of the accelerator is necessary. Upgrade of the detector has to be done not only to deal with much higher luminosity and background but also to achieve better performance. The physic programme will focus on several processes, already studied at the Belle; however the capabilities of the Belle II detector will cover full range of physics related to B mesons, charm quark, tau lepton and other physics in electroweak interaction region. An example of Belle related measurements is the study of decays of beauty quark into strange quark and photon where time-dependent *CP* violation was previously observed. Here a better resolution in silicon vertex detectors needs to be achieved. Also a purely leptonic decay of *B* meson into neutrino and tau lepton, discovered at the Belle will be further investigated. This will employ the electromagnetic calorimeter, especially in the high background conditions. In decays of B meson to kaon and pion, also studied at the Belle, the case with neutral final particles is a challenge for the calorimeter. But if neutral B meson decays into charged kaon and pion, separation between them is a task for the particle identification system and the vertex detector. These are just a few examples, for detail, see [5]. Individual detector parts are briefly described in the following chapter.

There are two main numbers which characterize ambitiousness of the Bell II experiment and SuperKEKB machine: instantaneous luminosity of $80 \times 10^{34}\mathrm{cm}^{-2}\mathrm{s}^{-1}$ and the goal of total integrated luminosity of $50\ \mathrm{ab}^{-1}$ in 2020. The SuperKEKB is located in the same tunnel as the former KEKB. The accelerator upgrade includes magnet and support systems and changes in several physical parameters of the machine. While the energy of electrons circulating in the High Ring (HER) is decreased from 8 GeV to 7 GeV, energy of positrons in Low Energy Ring (LER) is increased to 4 GeV from 3.5 GeV used in the KEKB. The beam currents are approximately doubled to 3.6 A in LER and 2.62 A in HER. The extreme luminosity is actually achieved by adopting the so called “Nano-Beam” scheme at SuperKEKB. This means squeezing the beams crossing at nonzero angle

just before collision so that the vertical beta function of the beams is significantly decreased. Value of this parameter is to be lowered from 5.9 mm to 0.27 mm in LER and 2.62 in HER which will lead to almost 40 times higher luminosity compared to that achieved at the Belle. [5]

The main concept of the detector remains the same as in the Belle experiment. The detector is a cylinder with a bit asymmetric internals which cover larger angle in the forward direction (direction of electrons travelling in HER). The key improvement of the detector is the replacement of the silicon strip detector near the interaction point by a pixel detector, where the strip detector follows just after the pixel one and occupies larger volume than in the Belle. The particle identification device is completely new and offers almost the best achievable separation between pions and kaons. Calorimeter is going to be upgraded by pure CsI crystals in the end cap and much faster readout electronics. While the barrel part of the muon detector remains the same, end cap is going to be equipped with scintillators instead of resistive plate chambers.

1.3 The Detector

Main source of detector facts in this subchapter, with many technical details, is [5].

The journey of particles created in collisions starts in the Interaction Region (IR), where at one interaction point beams are crossing at angle of 83 mrad. The beams are guided in two separate beam pipes, surrounded by focusing quadrupoles, of which three are permanent and five superconducting, and a system of compensation superconducting magnets to compensate for the detector's permanent field effects on the beams. Due to substantial focusing of the beams before collision and extreme luminosity, the Touschek intra-bunch scattering will play the most significant role in a beam background, especially coming from HER. Several other effects such as synchrotron radiation, scattering of the beams on gas particles in pipes or radiative Bhabha scattering will contribute. Because the first layer of the sensitive part of the Belle II detector starts at only 14 mm from the interaction point, a high background is expected to come also from low momentum (starting at about 6 MeV, slower will not reach the detector due to magnetic field) electron-positron pairs produced via two photon process arising from interactions of positrons and electrons in the beams. Since this is a quantum electrodynamics (QED) effect, it is

proportional to luminosity, which is going to be almost 40 times larger in comparison to that in the Belle. The other background effects are rather proportional to individual beam parameters which do not vary so rapidly.

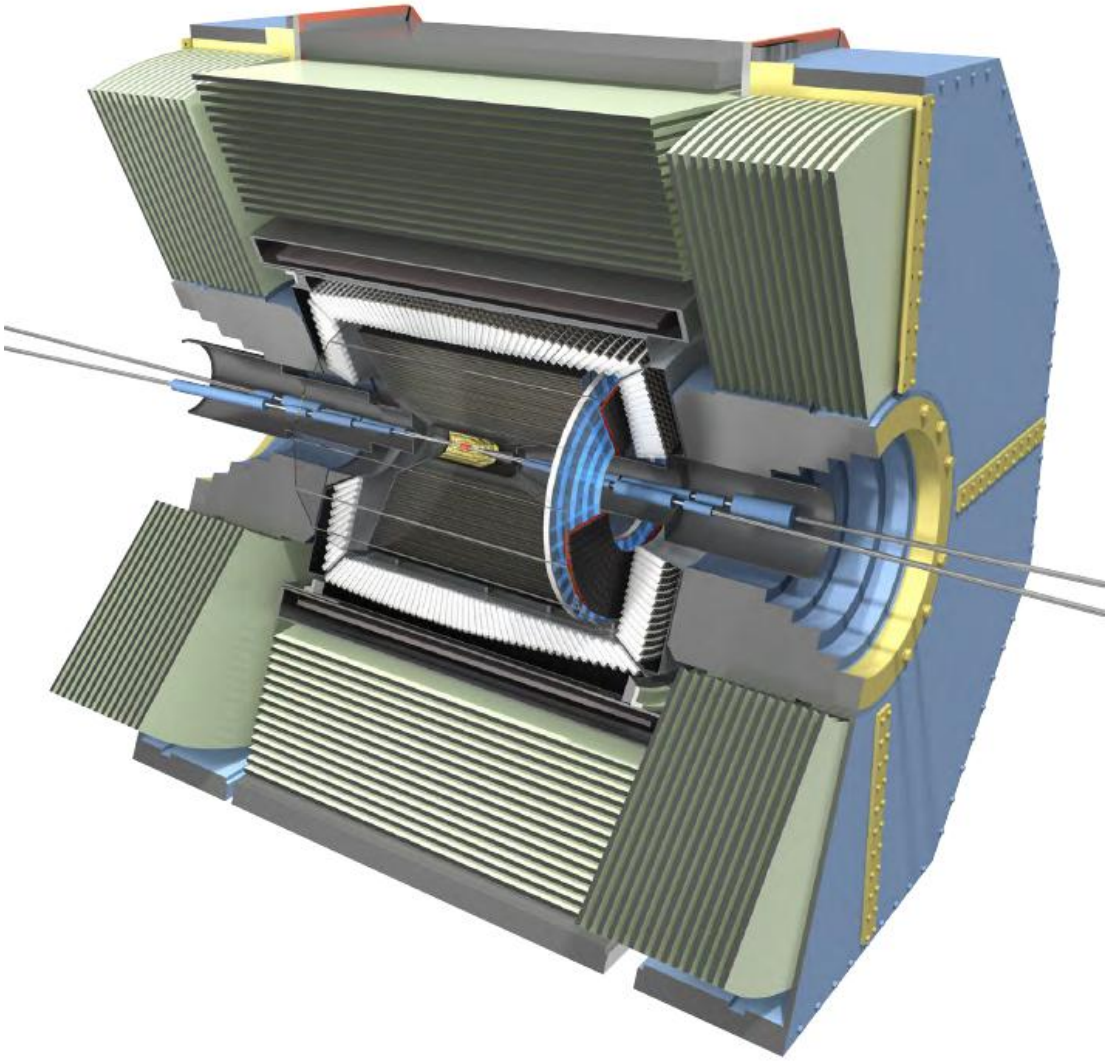

Figure 1: 3D model of the Belle II detector. From the center, there is small PXD in red, SVD in yellow, surrounded by CDC. ECL crystals are white. PID end cap is shiny blue and the PID barrel surrounds the ECL. Grey plates at detector edge belong to KLM. [6]

Due to expected occupancy, there cannot be a strip vertex detector used anymore for spatial reconstruction close to IR, as in the Belle detector. The Pixel Detector (PXD) is used instead. The actual layout consists of two layers surroundings the beam pipe placed at radii of 14 and 22 mm. Modules with width of 15 mm, 8 in the first layer and 12 in the second, have length of sensitive area 90 mm and 123 mm respectively. The sensors are arranged in a wind mill structure and cover the full acceptance angle of a particle tracker (part of the detector especially taking care of

vertex and momentum reconstruction and thus providing also first step in particle identification in magnetic field – formed from PXD, SVD and CDC, see below). To reduce multiple scattering in the PXD material, very thin sensor needs to be used and also the support construction and electronics needs to be reduced in the acceptance angle.

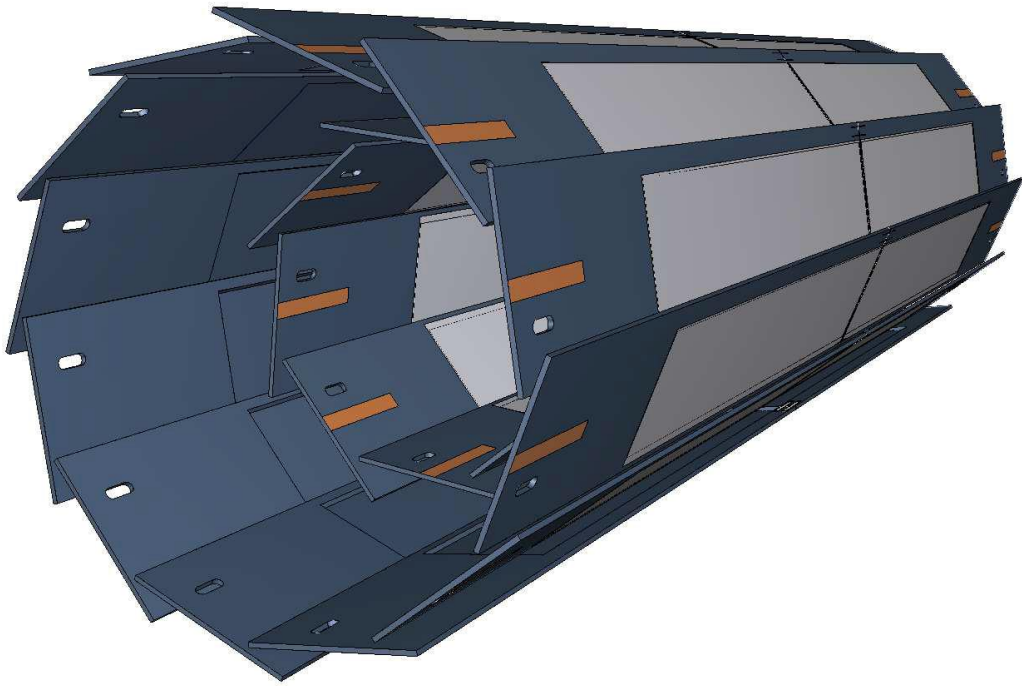

Figure 2: „Schematic view of the geometrical arrangement of the sensors for the PXD. The light grey surfaces are the sensitive DEPFET pixels, which are thinned to 75 microns and cover the entire acceptance of the tracker system. The full length of the outer modules is 174 mm.“ [5]

These requirements, together with needs for radiation hardness and performance parameters, altogether are fulfilled by the state of the art DEPFET technology. DEPFET, which stands for “DEPleted Field Effect Transistor”, is a pixel silicon detector with built-in pre-amplification in individual pixels. For more thorough description of the DEPFET technology and its operation, see following chapter. Thanks the in-place amplification, 75 μm thin sensors can be made without reducing particle tracking capabilities. Every sensor is inside a 450 μm thin silicon frame with switchers used for readout of individual pixel rows. Pixel sizes are 50 x 50 μm^2 in the first layer and 50 x 75 μm^2 in the second one. Readout electronics rests on the end of the sensor, outside the acceptance angle. The sensor itself consumes very little power and dry air cooling is sufficient. But the electronics needs

active cooling which is provided by evaporative CO_2 driven to the ends of the sensor by channels in the support structure.

Just above the PXD layers, from radius of 38 mm to 140 mm, there is a Strip Vertex Detector (SVD) formed from 4 layers with 187 double-sided silicon strip sensors in total. To reduce number of necessary sensors and to not have particles crossing SVD sensors at too acute angle, sensors in the forward direction are slanted to form a conical cap. In every pair of sensors, strips are parallel to the beam line on the inner side and perpendicular on the outer side, respectively. Individual silicon strip sensors have thickness of about 300 μm and a rectangular shape in the barrel region and a trapezoidal shape in the forward area. Thin sensors and special support structure are needed for mechanical stability and cooling without much increasing the material budget and thus not influence particles' tracks by multiple scattering. SVD covers the full Belle II acceptance angle. In reconstruction of tracks, it is important for connecting tracks from CDC and PXD together. It helps in elimination of the background in PXD and reconstructing tracks of low momentum particles which are not able to reach CDC. [5]

First massive (but lightweight) detection volume crossed by particles is the Central Drift Chamber (CDC). It is able to measure particles' energy losses and thus enables particle identification. As a part of the tracking detector, it also measures momentum and tracks with high precision and this information is combined with data from PXD and SVD to reconstruct tracks of charged particles. The CDC is filled by a gas (mixture of He and C_2H_6), where charged particles lose their energy and produce ions and electrons. A drift of created charged particles is induced by electric field among wires tense across the CDC. Two types of wires are present, sense and field. While sense wires serve as a signal source, field wires surround the sense ones are used to form an accelerating electric field. There are more than 42000 aluminium field wires, of which every nine form a single cell [7]. In the middle of the cell, there is the sense wire on positive voltage to attract electrons which have a higher mobility than ions produced by charged particles and thus a signal from them is present first. Among other purposes, CDC provides a triggering signal for charged particles and enables identification of particles which are not able to reach PID due to their low energy.

If particles have enough energy, they reach the Particle Identification Detector (PID) based on Cherenkov radiation, which is separated in two parts, a barrel along detector axis and end cap in the forward direction. The main purpose of PID is to distinguish between kaons and pions using momentum information from the tracker. In the barrel part, Time-Of-Propagation (TOP) counters with aerogel inside a quartz bar are placed around CDC. If a particle emits Cherenkov photons in aerogel, these are guided in the quartz bar thanks to internal reflexion and are registered at the end of the bar in a photon detector. Thanks very precise timing and very flat radiator walls, it is possible to reconstruct a partial Cherenkov ring image from time and two spatial coordinates. The end cap PID relies on proximity-focusing Aerogel Ring-Imaging Cherenkov (ARICH) detector, which consists basically from three parts. Cherenkov photons are produced in two 2 cm thick aerogel layers with slightly different refractive indices. Thanks that ring Cherenkov images produced along the aerogel layer overlap in the projection plane and provide better resolution due to minimizing emission point uncertainty. Between the projection plane and the aerogel layer, there is a 20 cm gap which allows Cherenkov rings to evolve and to be distinguishable with required resolution by photon detectors with avalanche photodiodes. [5]

To precisely measure energies of particles, especially photons coming from neutral pion decays, the Electromagnetic Calorimeter (ECL) is necessary. It is formed from 6624 CsI(Tl) crystals in the barrel region and 2112 pure CsI crystals in the end cap. Each crystal's axis is aligned so that it points toward the interaction point. As particle goes through a crystal, its deposited energy is converted into light output and registered by a photodiode at the end of the crystal. Pure CsI in the end cap is used because of its shorter scintillation decay time, however the light output is reduced by factor of ten in comparison to CsI(Tl). To get an additional internal gain, vacuum photo pentodes are used. Due to substantial increase in luminosity, an average occupancy of about 30 % is expected, so readout electronics with very fast processing is required, also because the ECL plays an important role in the triggering system.

The KL and Muon detector (KLM) lies outside the Belle II superconducting coil, its barrel region consists of eight layers of alternating iron plates and sensitive volumes. Iron plates serve as a radiator and return path for the coil's magnetic field

flux. Between every two iron plates, two glass electrodes Resistive Plate Chambers (RPC) are placed. In each chamber, two float glass plates covered by thin conducting layer on high voltages are separated by gap filled by a gas. While muons or kaons produce showers in iron plates, RPCs take care of registering and amplifying the signal from produced charged particles. Because of very high background, the end cap region of KLM is equipped by scintillators. Due to presence of the magnetic field, multipixel silicon photodiodes operating in the Geiger mode are used instead of photomultipliers. The scintillators themselves are long strips of doped polystyrene. The light from the scintillator is collected by an optical fibre and delivered to silicon photodiodes at its end.

To measure momentum of charged particles with high energies precisely, it is necessary to have an almost homogenous magnetic field with sufficient intensity inside the detector. This field is provided by a superconducting coil with intensity of 1.5 T bounding the ECL. The KLM besides just above the coil and its support structure together with iron plates serve as a return circuit for the magnetic flux. The coil itself is submersed in a liquid helium bath. The cryogenic system already present at the Belle is going to be reused with some components replaced or overhauled.

With the Belle II extreme luminosity, it is a challenge for the trigger to search in place for interesting events among other physical processes with higher cross sections. The trigger, operating at maximum average rate of 30 kHz, gets information from individual sub detectors and decides whether to readout detectors and send data to further processing. Several processes, especially triggered by ECL are used for precise luminosity measurement and calibration, because of their high rate. The main purpose is to trigger physically interesting events, such as decay of Υ resonance in pair of B mesons or tau lepton production. The main amount of data for readout is produced by PXD and SVD, so readout of these is triggered by outer detectors. While CDC delivers charged track information, ECL provides deposited energy information for both neutral and charged particles. For precise timing, trigger uses data from the PID. Finally the KLM gives information on muon tracks. All triggering data is collected in the Global Decision Logic (GDL), which then decides whether to reject a particular track or to accept it for calibration or further processing. Data from the GDL are processed by the Data Acquisition System (DAQ), where data size reduction is done and track reconstruction is performed in the high level trigger. The

software used in this trigger is the same as that used in offline processing. Actually, all data is formatted to ROOT objects at the very early stage and output of the DAQ is ready not only to be stored but also to be sent to server farms all over the world.

2. Silicon Vertex Detector

To reconstruct a collision event as close to its origin in the interaction point as possible, the "silicon" part of the Belle II detector is employed. Identification of primary and secondary vertices of particle tracks is needed for full kinematic reconstruction of the event. Also, full track reconstruction can be improved if primary vertex is identified. The vertex detector includes PXD and the innermost layers of SVD. Both of these detectors are based on silicon semiconductor technology, widely used in vertex detectors nowadays. Besides many technical and physical advantages (see below) semiconductor detectors benefit from radical development of commercial semiconductor devices in recent decades.

The layout of PXD and SVD is described in section 2.3. In following subchapters, some basic properties of silicon semiconductor detectors are given in a brief. The DEPFET technology for the pixel detector is described.

2.1 Semiconductor Detectors

This subchapter is mainly inspired by [8] *where one can find more detailed introduction to semiconductor detectors and related calculations.*

Silicon itself, as an element of IV group of the periodic table with four valence electrons, has many interesting properties. However, the most important application of silicon is based on so called doping, when atoms of elements with three (acceptors) or five (donors) valence electrons are incorporated into silicon crystalline lattice – one gets *p*-type or *n*-type semiconductor. While Silicon itself is a semiconductor, the number of electrons in a conduction band of a pure silicon crystal depends rather on temperature and is typically low. Doping can significantly change this situation. In *n*-type semiconductor, the fifth electron of the donor ends up in the conduction band. In *p*-type semiconductor, instead of electrons, we speak about holes, because one missing electron of an acceptor's valence band is taken from the lattice and there is a positively charged hole created in the conduction band.

Putting *n*-type and *p*-type semiconductor together, there is a so called *PN*-junction formed on the interface. Diffusion of charge carriers in both types of semiconductor leads to recombination of holes and electrons at the interface. The atoms of the lattice are no more shielded by conduction electrons at the boundary and

opposite charges are formed on both sides. Electric charge formed at the junction cancels the diffusion in the equilibrium – the region, where the charge of crystalline lattice atoms is not compensated, is called depletion area. A typical characteristic of *PN*-junction is that electric current flows along the junction only in one direction.

By applying an external voltage at the junction, the depletion area can be extended in whole volume of the semiconductor. Such a device can be used as a particle detector, where the depletion area serves as an active volume. Mean energy to create an electron/hole pair in the silicon is $3.65\ \mathrm{eV}$ which corresponds to small gap between conduction and valence band in the silicon lattice. If an electron/hole pair is created in the active volume, the field along the junction separates both carriers and their drift to opposite sides of the active volume. This results in a current flowing in the junction that can be detected by other techniques or, as in the DEPFET, released conduction electrons can be collected for some period of time directly in the semiconductor device.

Charged particles crossing silicon volume deposit energy through various processes. Ionization and excitation are basic effects common to all charged particles. These effects are also crucial due to low ionizing energy in a semiconductor – that means large amount of electron/hole pairs is created. For light particles, bremsstrahlung can play a significant role in particle's radiation loses. Another significant effect is high energy δ-electrons release caused by high momentum transfer from incident particle to electron in the medium. A precise computation of energy loses are nowadays a common task in high energy physics software, like Geant4. However simulation of charge collection and working of the semiconductor device is purely part of the newly developed basf2 PXD digitizer.

Almost whole volume of a fully depleted *PN*-junction serves as active area. A *p* or *n*-type semiconductor volume forming the junction, which is fully depleted, can be described as charge density ρ and the electric potential φ can be found by solving Poisson equation

$$\nabla^2\varphi = -\frac{\rho}{\varepsilon_0\varepsilon_{\mathrm{Si}}}, \tag{1}$$

where ε_0 is vacuum permittivity and $\varepsilon_{\mathrm{Si}}$ relative permittivity of silicon. Boundary conditions correspond to voltages on the edges of the semiconductor. The electric intensity

$$\vec{E} = -\vec{\nabla}\varphi \tag{2}$$

results (approximately in low intensities below ~ $10^4 \mathrm{V\ cm^{-1}}$) in velocity $\vec{v}$ of charge carriers

$$\vec{v} = \pm\mu\vec{E}, \tag{3}$$

where μ is charge carrier mobility (in silicon, different for holes and electrons) and the sign is plus for positively charged carriers.

During movement of charge, its spread is influenced by diffusion. This is caused by collisions of charge carriers with the medium. Similarly the carriers tend to move from areas with higher concentration to regions with low amount of charge carriers. These processes can de described by diffusion equation

$$\frac{\partial}{\partial t} n(\vec{r}, t) = D\nabla^2 n(\vec{r}, t), \tag{4}$$

where $n(\vec{r}, t)$ is conduction electron concentration at $\vec{r}$ and time t. D is determined by the Einstein relation for diffusion of charged particles

$$D = \frac{kT}{e}\mu, \tag{5}$$

where k is Boltzmann constant, T is thermodynamic temperature, e is elementary charge (for carriers with unit charge). The diffusion can be simply modelled as Gaussian smearing of size of an "electron cloud" traveling through the silicon.

All equations (1) to (4) can be significantly simplified by reducing number of dimensions to be taken into account. For a brief description of how this is done in the PXD digitizer, see section 5.3. Let's finally summarize properties and advantages of semiconductor detectors:

- Thanks quite high mobility of electrons and high level of integration, charge collection can be very fast. This property is crucial for Belle II high background environment.
- Low energy needed for an electron/hole pair creation ensures high number of charge carriers created and sufficient signal.

- Silicon serves not only for detection but thanks relatively high density allows also significant energy deposition even in thin layer of material.
- Mechanical stability of silicon allows radical thinning of active areas Additional internal amplification specific to DEPFET detectors (see next section) then ensures good response to incident particles even in thin devices.
- High-end semiconductor technologies allow high integration of readout electronics, create desirable in-pixel potentials by various doping techniques and tune the semiconductor device for particular use.
- Spatial resolution of semiconductor devices can be very good. In pixel detectors, typical size of an elementary cell, a pixel, is in 10's of micrometres. Diffusion effects allow charge sharing among individual pixels and thus advanced clustering algorithms can be used to further improve spatial reconstruction.

2.2 DEPFET Pixel Detector Briefly

The DEPFET (depleted *p*-channel field effect transistor) principle was introduced by Josef Kemmer and Gerhard Lutz in 1985. Since its invention, DEPFET has proved outstanding performance in many applications, ranging from optical photon sensors to X-ray imagers and particle trackers [9]. Integrated internal amplification in every single pixel and very compact in place structure with low capacitance offers very good signal-to-noise ratio, energy resolution and enables reduction of sensitive areas' thickness down to 75 μm.

A single DEPFET pixel consists of a p-channel field effect transistor which is integrated onto an n-type bulk with p-type contact on its bottom surface [5]. The transistor itself has three contacts, one serves a gate field controller, two as source and drain contacts. Considering the voltage of the source contact as zero level, the drain channel has negative voltage. The n-type layer serves as a detection volume and by placing a relatively high negative voltage to its bottom p-type contact, it becomes fully depleted. Just below the integrated transistor external gate, there is

another, an internal gate. It is formed by sideward depletion and additional n-type doping about 1 μm below the externals gate channel. Thanks that, the internal gate forms a potential minimum for electrons.

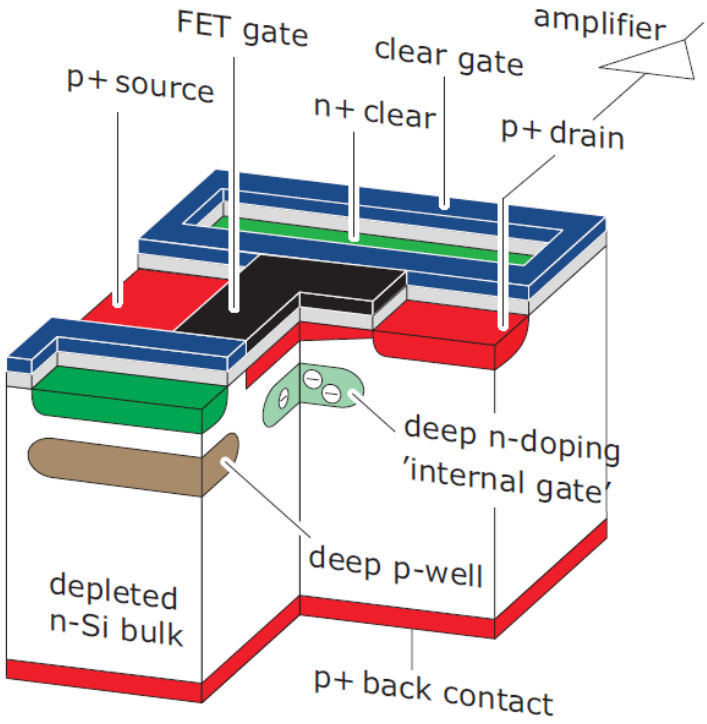

Figure 3: A schematic sketch of a single DEPFET pixel with the internal gate in the middle, just below the transistor channel. [5]

If a charged particle enters the depleted sensitive silicon layer, it deposits energy through creation of pairs of holes and electrons. At this time, the pixel is typically "off", which means small positive voltage is applied at the transistor external gate. Here comes the magic. The electric potential distribution causes that holes created in the detection region drift to the negative bottom side, while electrons are collected in the internal gate. If now the pixel is suddenly turned "on" by applying small negative voltage to the external gate, the current flowing through transistor channel to the drain is amplified by the charge collected in the internal gate. This process is called readout and can be repeated many times, because it has no influence on the charge collected in the internal gate. Electrons collected at the internal gate, together with those coming from thermal noise need to be removed from the pixel, typically just after the readout. This is realized by a clear n-type

contact integrated next to the gates. This contact has small positive voltage with respect to the source channel of the transistor during charge collection in the pixel. The clear region is shielded by a deep p-well, which prevents electrons traveling to the internal gate from ending up in the clear during charge collection. If charge removal is requested, clear contact voltage is significantly increased and all electrons are "sucked out" of the internal gate. Initial conditions are now restored and the pixel continues integrating generated charge until next clear signal.

The key parameter of the DEPFET sensor is its internal amplification g_q. It is defined as a transistor current response ΔI_d in drain channel to number of electrons collected in the internal gate

$$g_q = \frac{\Delta I_d}{e^-}. \tag{6}$$

This constant parameter is directly proportional to external gate conductance and indirectly to internal gate capacitance. The capacitance of the internal gate is very low and achievable values of the internal amplification reach $g_q \sim 560\ \mathrm{pA/e^-}$. Due to very compact structure of the sensor, almost no losses in created electrons occur, which together with low internal gate capacitance leads to a very low noise in the device and easy signal separation. Sufficient signal response enables radical thinning of the DEPFET sensor, which is essential in low multiple-scattering design used in the Belle II inner detectors. [5]

Another challenge is to manage operation over large matrices of DEPFET pixels and realize readout and clear procedure in a very short time and at a high rate. Readout is done in a parallel manner when four rows are read at once to minimize readout time in the Belle II DEPFET sensor, of which the longest have 1600 rows. Readout and clear process is invoked by the SWITCHER chips integrated at both long edges of the sensor. After activating the external gates, a signal current appears in the drain channels in every column and is driven by conductive channels along the sensor to its end. Here are the drain current digitizer chips (DCD) which convert the analogue signal into 8-bit number and send the result to the Data Handling Processor (DHP) chips. These devices provide signal processing and a zero-suppression. Because quite a large pedestal drain current is needed for DEPFET operation, this has to be subtracted prior to digitization to minimize data size. The pedestal removal

can be done by subtracting a cached value from the drain current in DCD or this can be achieved by so called double sampling: If clear signal is invoked just after the readout and second readout is performed, the DCD compares the two received values and returns only the signal part with constant pedestal removed to the DHP. Signal is also buffered and compressed inside DHP chips, after that it is send to the data handling hybrid outside the sensor and further to the DAQ. The overall readout cycle of whole matrix is manageable within only 20 μs. [5]

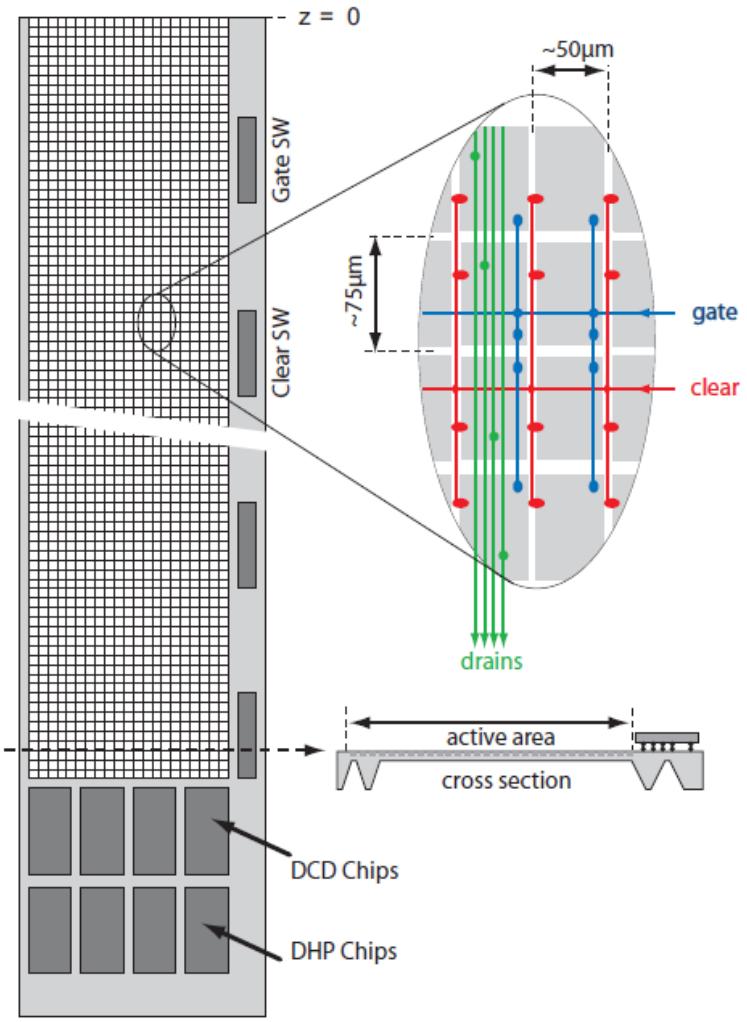

Figure 4: Single PXD module with DEPFET matrix and SWITCHER (SW), DCD and DHP chips visible. In the top right corner, interconnections for parralel readout are shown. [5]

In the Belle II conditions, especially in a distance of just a bit more than 1 cm from the interaction point, the DEPFET sensor will suffer from intensive radiation. Effects of irradiation include primarily a threshold voltage shift in the transistor, secondarily worsening of its amplification properties and higher noise. The voltage

shift can be however bypassed by changing the voltage applied to the external gates during readout. The DEPFET sensors are expected to withstand a dose of 10 MRad without significant performance decrease which could not be got around by changes in operation parameters or signal processing. [5]

3. The basf2 Framework

3.1 Introduction

A unified software framework for detector simulation and data analysis is a great advantage for contemporary high energy physics experiments. This is because of their unimaginable complexity and huge amount of data to be handled and accessible for physical analysis by collaboration members which typically come from all over the world. This also involves use of the most advanced IT infrastructure available. Required computing resources often exceed those available at individual institutions, therefore grid computing and resources redistribution is necessary. Thus the software used has to offer availability of parallel processing and unified input and output.

In 2010, development of the basf2 Framework began. It is a successor of the basf Framework (belle analysis framework) developed for the Belle experiment. The basf has been extended to "roobasf" with ability to operate ROOT files with parallel processing. Independently, there was the ILC framework with high integration of the pixel detector. Instead of merging these frameworks, it has been decided to develop a new one inheriting best patterns from its ancestors. Development of a new framework from scratch allows also possibility to use state-of-the-art techniques and to gain from software developed for recent physical experiments. [10]

The framework is used for both online and offline processing. Online means that it is fed by data coming from the detector trigger. As a part of DAQ, specifically the high level trigger, it performs full reconstruction and selection of physically interesting events. The reconstruction code is the same for online and offline processing, which is essential to keep consistency between experimental and simulated data. Offline processing takes care of high level data analysis and Monte Carlo production (simulation of large data samples). Precise detector description is required for Monte Carlo production and it has to be known also to the online layer for reconstruction. In the offline processing, complete simulation can be performed, together with simulation of detector response (known as digitization) and track recognition. This is necessary not only to verify experimental data but also to study detector performance prior to its construction. The basf2 Framework offers

everything discussed and much more, however it is still under intensive development and thus some features may be updated or added to further improve its capabilities.

3.2 Framework Overview

The framework runs on UNIX based systems and relies on several third party software projects, typically well maintained by large collaborations. C++ is used as the main programming language of the framework. The Python programming language is used for scripting, where appropriate. Both languages are a contemporary standard in high energy physics experiments and are natively object-oriented as the framework itself. The basf2 uses the ROOT data analysis framework [11] extensively, especially for data management. Simulation relies on the Geant4 toolkit [12] and many useful features from the HEP class library. The SCons software construction tool extends framework control over the build process and the boost libraries provide an extension to the C++ language itself. The third party software is called "externals" in the basf2 and the mentioned projects are not a complete list. [5], [10]

The key concept of basf2 is modularity. Together with unified data handling and ROOT capabilities, this enables basf2 to deal with the parallel processing in a surprisingly easy way. Modularity is essential, until no module is mentioned, nothing happens. To handle modules, Python steering is introduced. Python is a very powerful language, especially with the PyROOT extension, which unlocks all the capabilities of ROOT to use inside end user steering script. Python scripts are used to steer the framework efficiently, just by selecting modules to be used and setting their parameters, see below.

The basf2 is divided into several subsystems. The kbasf2 executes the modules in a so called path, while the pbasf2 is able to run many instances of kbasf2 in parallel. Another such subsystem is the gbasf2 which takes care of grid computing. In parallel processing, it is inevitable to provide a common data access interface. This interface is realized by specialized I/O modules. The framework automatically switches to parallel processing mode (pbasf2) after a single command in the steering script.

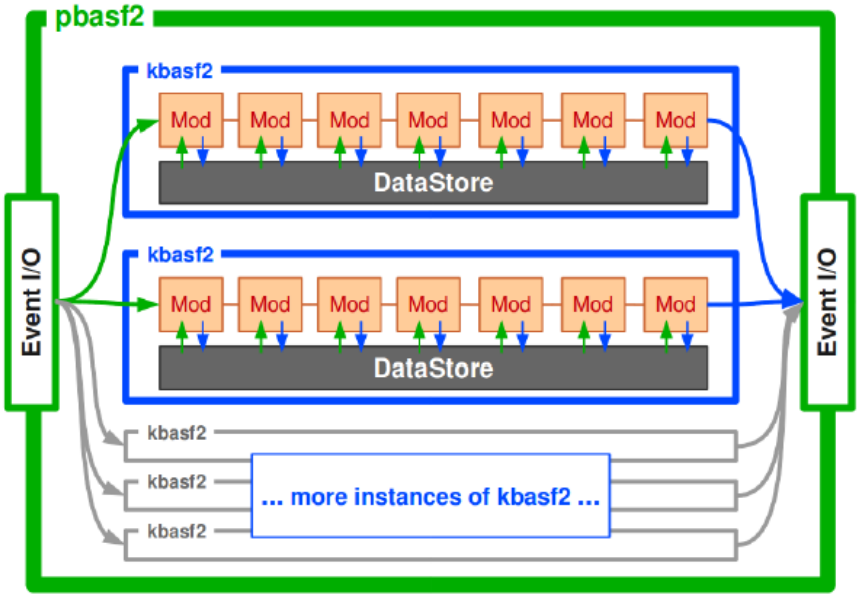

Figure 5: Subsystems of basf2 and illustration of common data access interface in parallel computing. [11]

The modules are the building blocks of the basf2 framework. Every module is a C++ class with a specific pattern. It inherits from an abstract base class, calls a macro returning an instance of a new module and implements several functions required by the base class. A module is controlled through parameters defined inside its constructor and set from the steering script. Some modules have special functionalities, for example they can trigger new event processing, enforce the framework to switch to single processing mode if the module does not support running in parallel, or contrariwise tell the framework that the module can read/write data from an event streaming server. Functionalities shared among modules should be placed into libraries instead. These libraries are auto-loaded by the framework. [10]

Modules are executed one by one in a path. Addition of modules to the path is realized in the steering script. Every module can return a value, which can be used in conditions switching to another path. From the paths and conditions, very complex processing structure can be build up. Reading and writing data to files is realized by specialized modules, which must be added to the path being executed. For example, a typical simulation scenario would require an event metadata module, a module to read and build up detector geometry, a particle gun and simulation module. Additional modules would include for example digitization, track recognition and further analysis. Anyone of the mentioned modules does not store anything directly

to disc. These modules store and read data with specified persistency into/from a common DataStore, which realization is hidden through abstraction. During the simulation, the output is controlled by another module which takes care of storing required data to the disc.

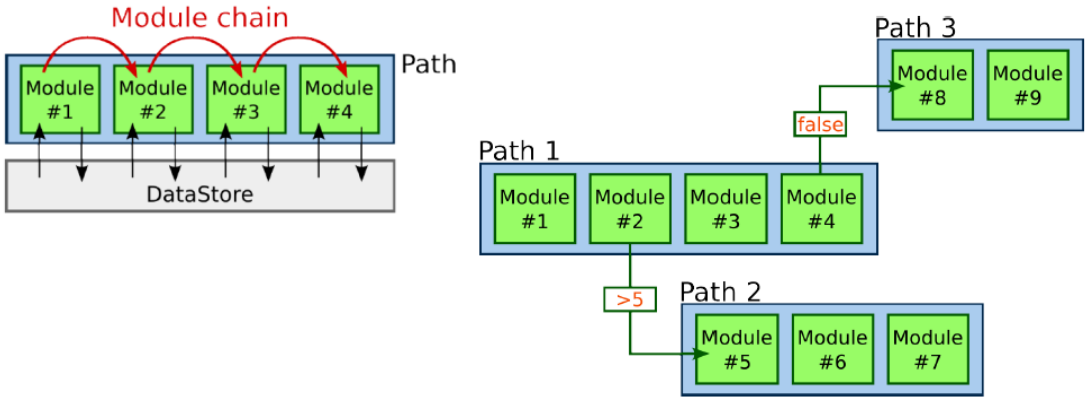

Figure 6: A simple chain of modules with common DataStore access (left) and example more complex processing structure built up from paths and conditions (right). [11]

All the data created during the event processing is managed by the DataStore. It is able to store any C++ class with ROOT dictionary and inheriting from TObject. Stored object have their defined durability, they can be deleted each event, each run or be kept until event processing finishes. From the module code, the DataStore is accessed via so called “accessor classes” which serve as templates expecting class name of desired object to be provided. The class name is provided in the declaration, where also name of the object or array of objects to be accessed has to be specified. The DataStore then automatically picks up an already existing object or it creates a new one. After that, the object can be accessed as usually and updating of the storage is done automatically when necessary. [10], [13]

For realistic simulation, knowledge of detector geometry is essential. The geometry is handled in a unified way in the basf2 framework. The main reason is that the software has to access the geometry information during Geant4 simulation, digitization or reconstruction, while different levels of geometry description are required in these steps. To avoid redundancy in geometry definitions, the parameters describing geometry are stored centrally in a parameter repository [13]. The parameter repository keeps values in XML files describing the geometry in a tree

structure. While the digitization is supposed to access the repository directly (through GearBox geometry handler, see below), Geant4 simulation and latter reconstruction rely on full geometry with all C++ objects representing logical and physical volumes stored in the memory. To create these objects, C++ classes called “Creators”, are incorporated. The creators are similar to modules, but are auto-loaded by the framework according to content of the geometry XML document, not the steering script. These creators are called by a geometry builder module, while it is reading the main file with geometry specification. [13]

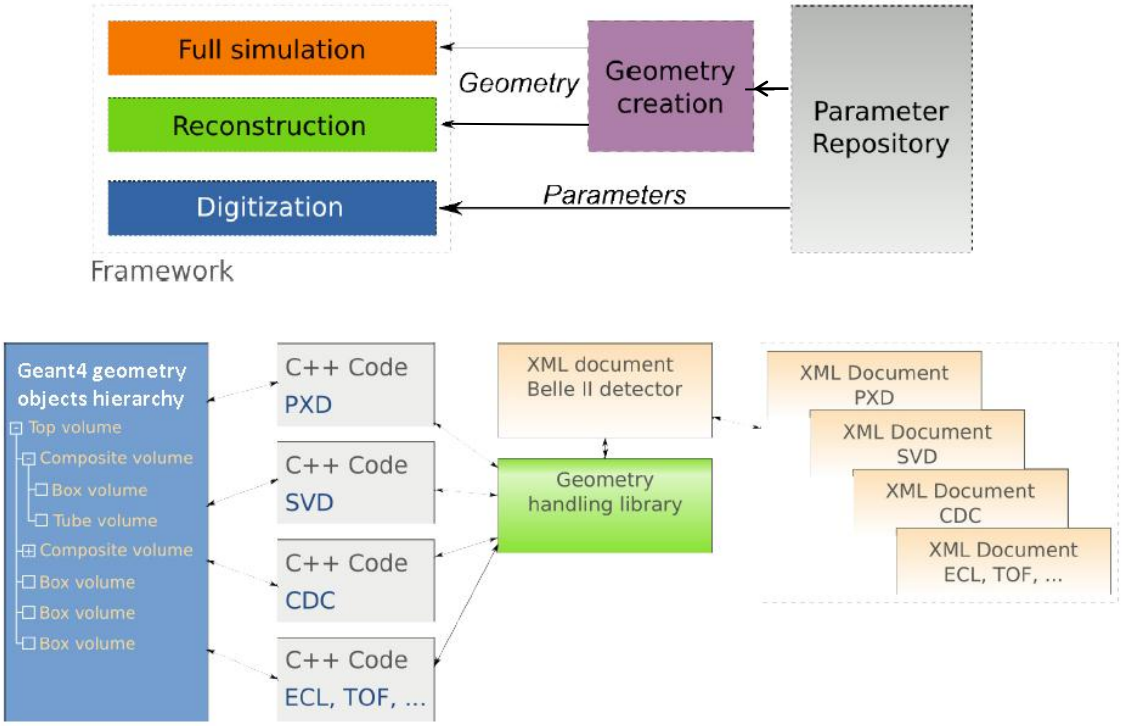

Figure 7: Concept of common geometry usage in the framework (top) and Belle II detector geometry building (bottom). [10]

The main XML document consists of several parts, typically located in different files included in the XML, which have specific creators assigned. Each sub detector in the Belle II has for example its own creator or there is a creator for materials used. For access to the XML structure, a geometry handling library is used. This library provides an abstraction over actual data retrieval mechanism through several classes, like GearBox (for general parameter access) or GearDir. The GearDir object is passed to a creator, which uses it to loop through the tree parameter structure. After reading parameters, appropriate Geant4 volumes with specified dimensions are created and positioned inside their mother volumes. This tree

hierarchy for a sub detector is then passed to GearBox singleton which adds it to a world volume. Volumes intended to be “active” are connected to their assigned handlers, so called sensitive detector classes. These objects similar to modules are called by the simulation module as Geant4 is stepping through active volumes. The finished geometry is stored centrally in the memory and can be accessed from anywhere in the framework.

Prior to the simulation module, there is typically a particle gun module in the path, which belongs to so called generators provided also by the framework. Other generators are used typically in background simulations. The simulation is driven by a simulation module and supported by a simulation library. The detector geometry is passed to Geant4 for particle tracking and data created by particles going through sensitive volumes are stored to the DataStore by the sensitive detector classes in every step. Geant4 provides only spatial information on particle tracks and energy deposited in individual steps. Event data from the simulation module are usually processed in digitization modules to gain simulated detector response. Further modules might provide clustering, track recognition and further analysis.

4. The Beam Test & Geometry

The DEPFET detectors are regularly tested in real conditions at particle accelerators in so called **beam tests**. Beam tests allow understanding DEPFET properties in high energy conditions and to analyse detectors' spatial resolutions, select best readout methods, operation voltages and other parameters, evaluate response of irradiated sensors and train the personnel. Also the whole infrastructure, like online monitoring, data acquisition, powering, cooling etc. is a subject of beam test studies. Analysis of beam test results is crucial to evaluate detector properties and validate tools, like device simulations.

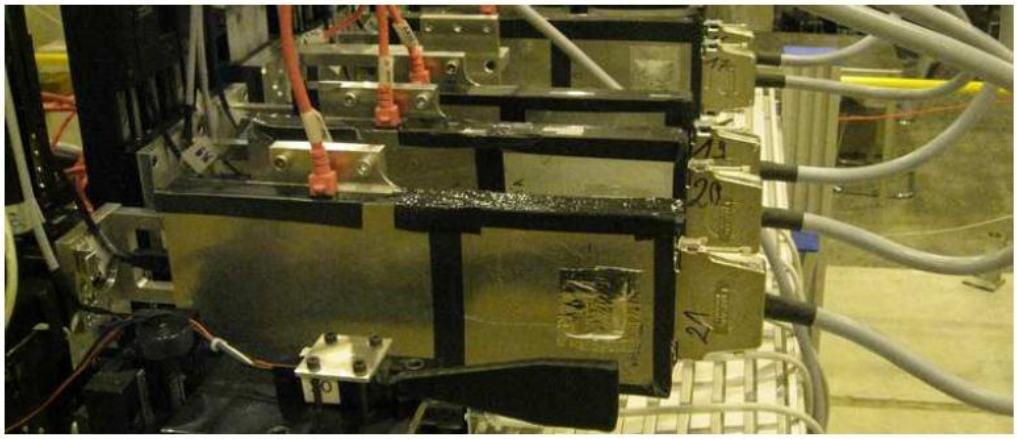

Figure 8: „A photo of the DEPFET beam telescope in the H6 experimental area at the CERN SPS." [5]

The setup of the beam test simulation reproduces conditions in the experimental beam test of ILC[3]-type DEPFET matrices performed in 2009. The experimental beam test was conducted at CERN in experimental area H6 and complete analysis results can be found in [14].

The ingredient part of the simulation is precise geometry conditions reproduction and possibility to simply change geometry conditions through XML files. Simulation also allows evaluation of multiple scattering contributions and with known experimental results from 2009 it provides a way to validate beam test simulation in basf2 itself. In second simulation scenario, there will be the evaluated

[3] International Linear Collider, proposed experiment for which the DEPFET is planned for a vertex detector. For Belle II thinned sensors have been developed.

"thick" 450 µm ILC-type sensor replaced by 75 µm thin Belle II type DEPFET matrix.

4.1 Geometry Specification

The basic layout of the geometry is shown in the Figure 9. It consists of six modules positioned in the beam line. In the experiment, the third sensor served as the detector under test (DUT) while the other five sensors were used as telescopes (TEL). Individual sensors are placed at exact positions in the beam direction. The z-coordinates refer to middles of the DEPFET matrices. Remaining coordinates lie in sensor planes, while y points towards up and x "to the right", as shown in the Figure 9. The origin of the coordinate system is located in the centre of the first DEPFET matrix and the particle gun is placed a few millimetres in front of it during the simulation.

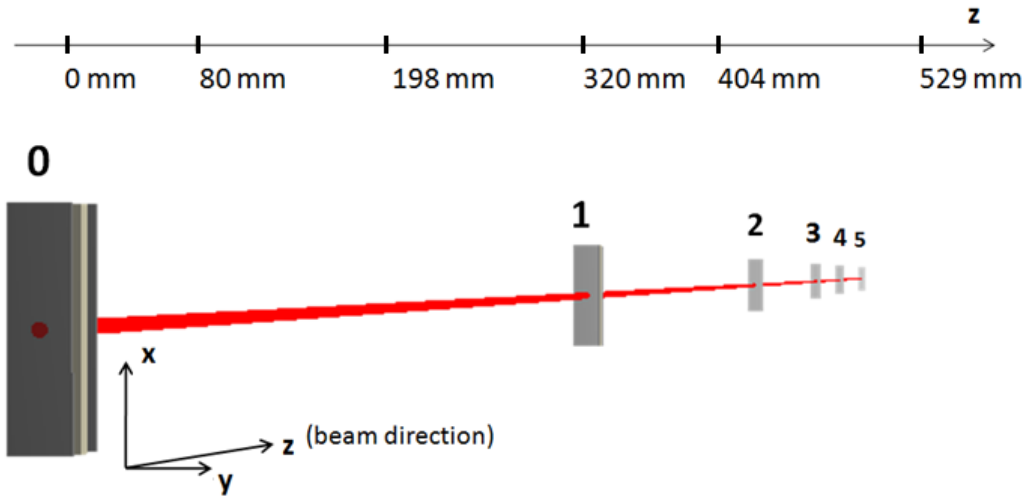

Figure 9: Basic geometry layout in the beam test simulation. Origin of the coordinate system is in the center of the first sensor. Positions of individual detectors are shown (top).

Each module is formed from a 450 µm thick silicon DEPFET matrix surrounded by two aluminum foils with thickness of 100 µm, see Figure 10. All sensors' matrices have the same number of rows and colums: 256 x 64.Two kinds of matrices with slightly different dimensions and pitch are used in the beam test simulation. While telescopes have pixel pitch of 24 x 32 µm, the ILC DUT has pitch of 20 µm in both directions and thus is a bit smaller. Belle II matrices placed at the position of the DUT in the second simulation scenario has larger pixels, its matrix

size has been choosen to be a bit smaller than telescopes. Sensors' parameters are sumarized in Table 1.

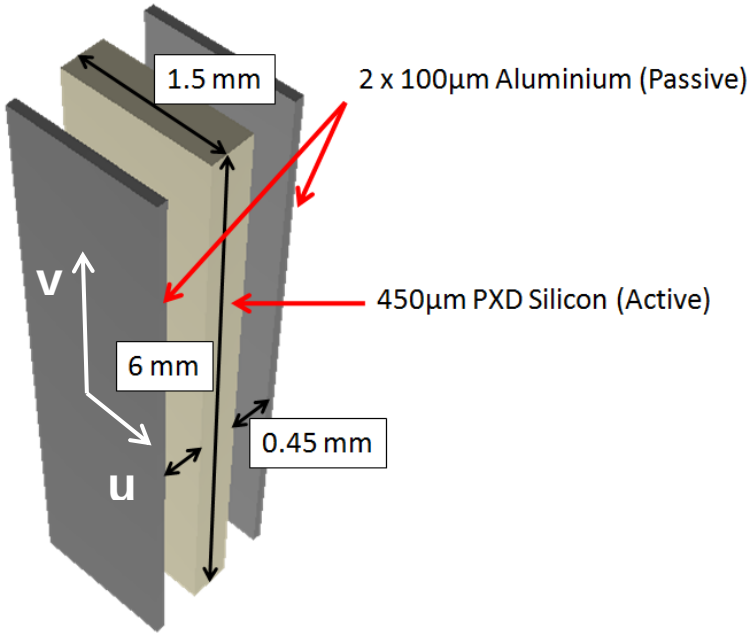

Figure 10: A single module of the ILC type (not thinned). Dimensions are approximate and slightly different for each sensor type. See Table 1 for exact values. The local coordinate system [u, v, w] (with origin in the middle of the sensor and *w*-coordinate pointing towards back) is shown in white.

Module #	X-position [mm]	# Cells	Pitch [µm x µm]	Dimensions y/z/x [mm]	Remark
0 (TEL)	0	256 x 64	24 x 32	6.144/2.048/0.45	ILC pixel
1 (TEL)	80				
2 (DUT)	198		20 x 20	5.12/1.28/0.45	
		100 x 25	50 x 50	5.0/1.25/0.075	Belle II pixel
			50 x 75	5.0/1.875/0.075	
3 (TEL)	320	256 x 64	24 x 32	6.144/2.048/0.45	ILC pixel
4 (TEL)	404				
5 (TEL)	529				

Table 1: DEPFET matrices parameter in the beam test and different DUT's used in the simulation. Number of cells for the Belle II matrix has been chosen so that the DUT is a bit smaller than the telescopes.

For realistic simulation, individual detector matrices cannot be perfectly aligned. But adding detectors' small random offsets by hand in XML parameter file (even separated) would be annoying. By doing this automatically during geometry building, we would lose control over the offsets' values, because the geometry creator classes are called from geometry builder and cannot be steered from outside. This issue is resolved by setting small random offsets (or certain values) from the steering script and storing them into DataStore by a simple offset steering module (TBOffsetSteer). Offsets are added to ideal sensor positions during geometry building. The analysis module retrieves actual sensor positions from the geometry constructed in memory, see section 6.2.

Studied offsets partially follow that observed and analyzed in [14]. That includes small shifts in the detector planes and a slight rotation around the beam axis. Specifically:

- Displacements in y and z direction are set in range of ±30 μm.
- Rotation of the sensor plane includes shifts within range of ±7 mrad.

4.2 Geometry XML

All necessary parameter required to build the beam test geometry are stored in XML files. Processing of these files is a job for the GearBox module, which expects name of the main geometry XML file as a parameter. Once all XML files are processed and parameters are stored in the GearBox object, the geometry is ready to be created in memory. The geometry XML files are structured in subsections, each in separated file included in the XML. Each subsection code contains a "Creator" tag, which specifies the class able to understand the parameters and build appropriate Geant4 geometry objects and place them at desired positions inside the world volume.

The main geometry file, SimpleGeometry.xml, links a materials definition file and a file with some global parameters (GlobalParams.xml) served by framework creators. Last inclusion refers to the "sub-detector" file, which creator has been developed from the scratch for the beam test simulation. In case of Belle II detector geometry, all subdetectors (like PXD, SVD, CDC, etc.) are stored in separated files with different creators. The actual file structure is hidden to the developer during

geometry creation thanks that the access to the parameters is unified in the GearBox object. In the GlobalParams.xml file, the world volume dimensions and its material (air) are specified. All materials used in the simulation have to be defined in the TBMaterials.xml file. Any material specified has to be placed into Mixture node with name provided. A mixture can consist of one or more elements, of which everyone has a weight attribute representing relative amount of that element in the mixture.

The actual beam test geometry is defined in TBGeometry.xml file. Between the content tags, there are stored the parameters later passed to the class specified in the creator tag and discussed in following chapter. The XML code inside the content node consists of containers, which can be positioned relatively to the global coordinate system. In a container, two kinds of children nodes are allowed, one representing passive and the other active volume. The volumes are positioned relatively to the local coordinate system of their parent container. Containers and volumes must have position (three spatial coordinates and three Euler angles for rotation) and shape with its dimensions specified. Every node needs also to have tags with name and material. The containers need to have the same material as the world volume (which means air) to be invisible for tracking. Invisibility in geometry visualized by ROOT is set in the creator. On the other hand, active and passive volumes have a “Color” tag, which is used in geometry visualization.

The active volumes need to fulfill several additional requirements. First, they need five additional tags. The “SensorID” tag defines sensor index used in geometry navigation. Four remaining tags define sensor pitch and number of cells in both directions. These values are used during digitization and clustering of the DEPFET sensors. The name tag is very important for active volumes. It must have a specified prefix, “SD_” to be marked as “Sensitive Detector” during geometry conversion from ROOT to Geant4. The name tag also has to contain two substrings: “PXD” and “Silicon_Active”, because this is used in some geometry helper classes used by PXD package during simulation and digitization.

4.3 The Geometry Creator

The building of the beam test geometry is maintained by the TBGeoCreator creator developed for the beam test, which can handle objects of limited level of complexity, but is sufficient for our simulation and might also be adopted by other

basf2 (primary PXD) developers who need to use framework capabilities in simple geometry conditions.

A creator shares a similar pattern like a module. It inherits from CreatorBase class and implements constructor and “create” procedure. In the creator constructor, the prefixes in names of active volumes are connected to appropriate sensitive detector class using a function of the base class.

In the “create” procedure, the creator receives a GearDir object representing the parameter tree structure in the content tag in the XML. It reads its content by specialized functions and navigates through it using XPath expressions. After container parameters are loaded and related TGeo object is created, processing inside the creator continues with passive and active volumes inside. While processing the active volumes, pitch and matrix size is stored to a specialized object attached to the generated TGeoVolume. This object is also populated by the sensor index read from XML parameters. Active and passive volumes are positioned inside their containers according to the XML parameters while adding a new node to the container TGeoVolume.

After all volumes are created and placed inside their mother volumes, the containers are added to the subdetector volume created by a base class function. Their position parameters are updated by the offsets from the DataStore, if they are loaded successfully. As mentioned before, the offsets are stored to the DataStore by a simple module, called “TBOffsetSteer”. This module stores a single C++ object with offsets defined in the steering script into the DataStore.

5. The Simulation

5.1 Particle Gun and Simulation Scenarios

For particle generation, the basf2 PGunInput module is employed. It allows generation of single particle or a number of particle tracks in an event. For the beam test simulation, one track per event is produced. The particle gun module is steered from the script and allows customization of particle energy, gun position (particle production vertex) and direction in which particles are produced. These parameters can be set to certain values or be randomly chosen from Gaussian or uniform distribution.

In the experimental setup at CERN's SPS, mainly protons and pions were produced by the SPS accelerator. The primary setting of particles momentum was 120 GeV/c, but an energy scan was conducted also for lower energies. Separately, the experiment has been reproduced with electrons. Because results discussed in [14] concern mainly about pions and electrons, these particles belong to the basic setup of our simulation. Basic simulation scenarios include following settings of the particle gun:

- Pions with momentum of 120, 80 and 60 GeV/c
- Electrons at 100, 80 and 60 GeV/c
- Coverage of the whole DUT area by incident particles (at least) by setting uniform range of production vertex in y and z direction
- Beam divergence with Gaussian distribution (sigma 1.5 degrees in particle production angle)
- One primary particle per event

For analysis of the Belle II PXD detector, this will replace the ILC-type DUT from beam test 2009 simulation. Telescopes will remain the same. Next to the scenario with 120 GeV/c particles, a simulation with 2GeV/c electrons typical for Belle II conditions will be conducted. Finally an angle scan with this lower energy will be done for the Belle II matrix.

5.2 Particles with Wings

The simulation itself is controlled by the basf2 simulation module (FullSim module). It executes basf2 classes which wrap Geant4 user initialization and action abstract classes. The simulation module takes care of several important steps required before any particle can start its journey. These steps follow just after obtaining the Geant4 run manager instance and include:

- The detector construction which means passing the geometry already constructed in memory to Geant4
- Preparation of the physics lists which contain all physical processes the particles can undergo in the simulation
- Initialization of the magnetic field in the Belle II simulation, not present in our simulation
- Setting the primary generator action which takes particle list for an event generated by the particle gun to pass it to Geant4 tracking system
- Initialization of several other basf2 classes in the run manager for additional control over the simulation workflow

The Geant4 toolkit is based on Monte Carlo simulations with random sampling of the cross sections of processes defined in the physics lists. Besides that, Geant4 takes care of tracking the particle in steps with controlled length based on simulation preciseness and actual material properties near the particle position. It also computes influences of possible electromagnetic fields and; what is of highest importance; it computes particles' energy loses in the detector material. If the particle is unstable, its decay is also controlled and any descendant particles are tracked by the toolkit. Geant4 is very complex software with high level of documentation, best starting point is its web [12].

During the simulation, particles are tracked through the geometry until a sensitive volume is reached. The appropriate sensitive detector class is now called and an object with Geant4 step data is passed to it. The class provides storing of the "hit" data of the step and its relation to the particle. This class is available in the basf2 framework (in the PXD package) and is fully adopted in the beam test simulation. Particles are tracked until they decay, stop in the material or reach the

boundary of the world volume. After tracking of all particles generated by the particle gun and their decay products finishes, the simulation module job is done and this is a time for the modelling of the detector physical response, called digitization.

5.3 Digitization and Clustering

The finished Geant4 simulation leaves simulation hits in DEFPET matrices (PXDSimHit) in the DataStore. But to gain real detector response, it is necessary to simulate electron collection at the DEPFET internal gates, add noise signals and digitize the analogue readout signal in a single pixel. This process is realized by the basf2 PXD digitization module (PXDDigi). After the signal from all pixels in a DEPFET matrix is known, the pixels that belong to single particle are joined to a cluster in the PXDClusterizer module. After the clusters are formed, they are turned into "PXDHits" which represent the matrix response to a single incident particle[4].

The digitization module starts with some initialization and retrieving data produced by the simulation. It loops through all simulation hits in each sensor and retrieves sensor related data from geometry helper classes and matrix properties (pitch and number of rows/columns) stored during geometry building. Every simulated hit has its starting and ending point. The particle track is approximated by a line between these points and divided into smaller segments. The digitizer splits total deposited energy in the hit converted to number of released electrons among these segments – ionization points. Next step is charge drift simulation,

Charge collection is separated into motion to readout plane under influence of an electric field drift. In the readout plane, a random walk simulation of charge only due to diffusion is done. Approximation of vertical drift assumes constant doping concentration in the pixel. This results in a parabolic potential distribution from which electron drift time can be calculated. As a parameter to this computation, there enter the voltages on top (front) and back side of the pixel, sensor thickness and a parameter called "gate depth", which is the distance where electrons are assumed to reach the readout plane, where diffusion is simulated (it is actually the depth of the readout plane). Once drift time is obtained, the position of electron cloud arriving at the readout plane is smeared due to diffusion. Next step is electron cloud diffusion in

[4] If more particles hit the matrix so close together, that they cannot be distinguished, the hit is associated to all contributing particles through the Cluster relations in the DataStore.

the readout plane (without drift). Each electron cloud is divided into groups of electrons of size $\sim 50\, e^-$ and these are tracked separately. In each step the group of electrons is checked, whether it is inside internal gate (IG) or not. If not, its position is smeared by a Gaussian distribution with variance σ in each direction in the readout plane. This is equal to mean diffusion distance during the simulation time step Δt

$$\sigma = \sqrt{2D\Delta t}\,, \tag{7}$$

where diffusion constant is determined by (5). Electron groups are tracked until they reach any of the internal gates in the matrix or the maximum number of steps is reached. Remaining clouds are assigned to an IG according to their current position. Actual location of the IG and its dimensions are determined by three constants, depending on the pixel type. A symmetric border from left and right belongs to clear region (see section 2.2), width of the drain and source region limits vertical location of the gate. See Figure 11 for illustration in case of ILC pixels. This figure also shows the region where no charge diffusion in the readout plane is done and electrons are automatically assigned to the IG. All DEPFET matrices in the simulation use a double pixel structure, shown also in Figure 11, therefore the source and drain borders are switched for even pixels in the vertical dimension. Values used for the digitizer are summarized in Table 2.

In the readout simulation, the digit charge (charge in the IG) is smeared by Poisson distribution and Gaussian smearing is applied for electronics effects. The digits are then zero-suppressed and random noise digits are added to the digit map. The result of DEPFET matrix digitization are digits (PXDDigits) stored with relation to the particles, which produced them.

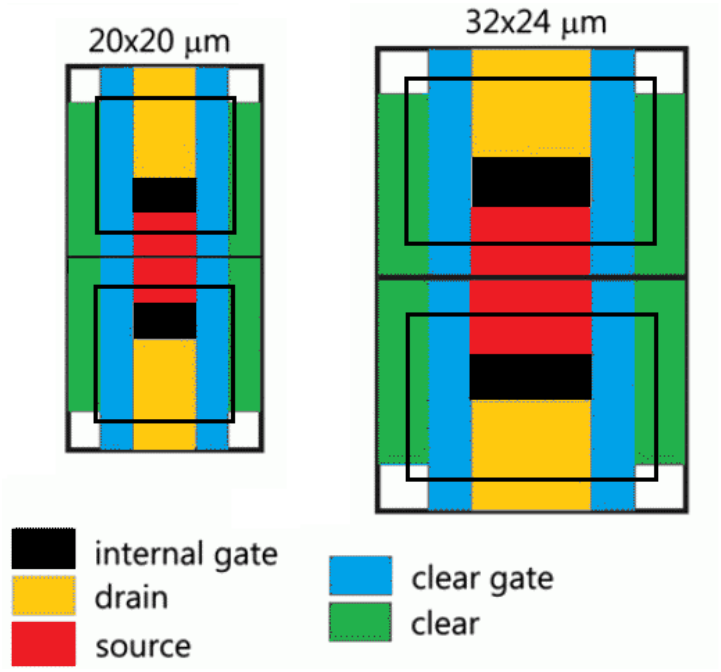

Figure 11: DEPFET ILC pixel structure, double pixels are shown. Small DUT double pixel is on the left, larger TEL type pixel on the right. The black frames inside each pixel approximately (see Table 2 for exact values) show the area, where no random walk simulation of the diffusion is done in the readout plane and electrons are assigned to the internal gate (in black) inside. *Taken from* [15] *and slightly modified.*

Parameter / Pixel type and pitch [µm x µm]	ILC 20 x 20	ILC 24 x 32	Belle II 50 x 50	Belle II 50 x 75
Clear border [µm]	3	3	8	8
Source border [µm]	3	3	3	3
Drain border [µm]	3	3	8	15
Gate depth [µm]	2	2	22	22
Back voltage [V]	-180	-180	-60	-60
Bulk doping [10^{12}cm^{-3}]	0.85	0.85	10	10

Table 2: Parameters for PXD digitizer charge collection simulation. Values for Belle II pixel are taken from the basf2 framework. *Parameters for ILC pixels come from B. Schwenker.* [16]

In the PXDClusterizer module, clusterization and hit reconstruction in the DEPFET matrix is done. The clusterizer loops over all digits in individual sensors and merges neighbouring digits around seeds[5] with signal above a threshold into cluster structures. The clusters are converted into hits (PXDHits) which requires estimation of the hit position from the charge distribution over the cluster structure. Position of the hit is calculated with centre of gravity algorithm for two pixel clusters or analogue head-to-tail algorithm for larger clusters. Hit is placed to the centre of the pixel in case only one digit contributes to the cluster in one dimension. Final position of the hit in the sensor, its total charge collected and relations to cluster and contributing particles is saved to the DataStore.

In the beam test simulation, some parameters of the digitizer and clusterizer have been studied for their contribution to the analysis results. The modules are designed for Belle II detector conditions and some minor changes to default parameters are necessary, they include

- Turning off the Lorentz shift present in Belle II magnetic field
- Adjusting the signal-to-noise ratio to correct electronics noise (in units of equivalent noise charge - ENC) to values applicable to DEPFET matrices, that is:
    - 290 ENC for ILC matrices in 2009 beam test. [16]
    - 200 ENC for Belle II matrices – default setting of basf2 PXD digitizer.
- Usage of advanced drift model in the Digitizer with random walk charge collection simulation, described above.

[5] The seed is the pixel with highest signal (that means collected charge – the seed charge) in the cluster.

6. Analysis

6.1 Analysis Outline & Exclusive Residuals

In the analysis, we need to get six crossing points of a particle track with the sensors in the beam test. Only tracks crossing all sensors are selected for further analysis. For these tracks, following steps need to be performed:

- Get coordinates of simulated and digitized (and clusterized) hits in sensor volumes
- Transform the coordinates to the global coordinate system
- Fit particle tracks with lines, once for simulated and for digitized space points
- Calculate exclusive residual for all sensors
- Retrieve cluster size, cluster charge and seed information from clusters
- Perform additional analysis of generated data in histograms

A crucial assumption for linear fit is straight track approximation. This is fulfilled both by low amount of scattering material and high momentum of primary particles (see section 5.1 for simulation scenarios). Evaluation of multiple scattering contributions to residuals is part of the analysis and is discussed later.

The most important step of the analysis is residual calculation. Because the level of multiple scattering influences on particle tracks is in micrometre range and DEPFET resolutions are just above, subtle effects appear, not being such important at worse spatial resolutions. Therefore it is a more precise approach to compute exclusive residuals instead of inclusive. The only change is that the track fit for a given sensor is computed only from the remaining sensors data. The studied sensor itself is not included in the linear fit. When it comes to residuals evaluation for that sensor, its hit position is compared to that predicted by the excluded fit. This ensures that the track prediction for the sensor is independent of the hit position it is compared to. As a result, the fit prediction is influenced only by the telescope

system[6] and presence of the evaluated sensor as a scattering plane in the beam test simulation.

The differences between a predicted and a measured space point for each detector form a covariant matrix of residuals. This matrix is almost diagonal at high momentum of incident particles, as the non-diagonal elements come from the multiple scattering. *Diagonal elements of the matrix are then equal to squared contributions of measurement error of the detector, of prediction error of the linear fit, and of multiple scattering* [17].Thanks to the exclusive residuals, these three contributions can be rewritten into sum of squared detector resolutions and squared resolutions of the whole telescope system (withou the studied detector). This analysis deals only with the diagonal elements of the covariant matrix of residuals. The linear fit is computed from formulae resulting from simple least squares method. Actually, due to exclusive residuals, every sensor has its own "track fit" derived from the other ones. The fitting and residual calculation is done independently in xz and yz plane.

If we get crossing points $\{(x_0, y_0, z_0), (x_1, y_1, z_1) \dots (x_{n-1}, y_{n-1}, z_{n-1})\}$ for n sensors in a given track, the excluded fit

$$y^{(i)}(z) = a_y^{(i)} z + b_y^{(i)}, \;\; x^{(i)}(z) = a_x^{(i)} z + b_x^{(i)} \tag{8}$$

for i-th sensor in the *y*-coordinate is calculated using [19]

$$a_y^{(i)} = \frac{(n-1).ZY - Z.Y}{(n-1).ZZ - Z.Z}, \quad b_y^{(i)} = \frac{Y.ZZ - Z.ZY}{(n-1).ZZ - Z.Z}, \tag{9}$$

where

$$Z = \sum_{j=0,\, j\neq i}^{n-1} z_j\,, \;\; Y = \sum_{j=0,\, j\neq i}^{n-1} y_j, \quad ZY = \sum_{j=0,\, j\neq i}^{n-1} z_j\, y_j, \;\; ZZ = \sum_{j=0,\, j\neq i}^{n-1} z_j^2\,. \tag{10}$$

Note that in all sums $j \neq i$. Analogically for $a_x^{(i)}$, $b_x^{(i)}$.

Exclusive residuals for i-th sensor are then given by

$$\Delta^{(i)}{}_y = \sqrt{\langle \left(y_i - y^{(i)}(z_i)\right)^2 \rangle}, \;\; \Delta^{(i)}{}_x = \sqrt{\langle \left(x_i - x^{(i)}(z_i)\right)^2 \rangle}, \tag{11}$$

[6] By telescope system, we mean here all sensors except the evaluated one.

where $\langle ... \rangle$ denotes mean value over all tracks included in the analysis. Exclusive residuals are in fact obtained as the parameter σ of a Gaussian fit performed on the data given by the expressions inside big round brackets in (11)[7].

6.2 The Analysis Module

The analysis module (TBAnalysis) has been developed from the scratch. In the event processing, the module first initializes connections to the DataStore. A loop through all relations of the particles to simulated and digitized hits is done and a structure containing all hits related to the particle and sorted by sensors indices is filled. The structure is searched for good tracks, which left hits on all six sensors.

The analysis continues with a loop over all tracks marked as good for both, simulated and digitized hits. Inside this loop, hits inside every sensor are examined. There are typically more simulated hits in a sensor that correspond to Geant4 steps. Only first and last hit in a sensor is taken and their coordinates are averaged. The same is done to the digitized hits; however the digitization should produce only one hit per sensor and particle, so this just for sure.

Before fitting, the coordinates of hits are updated to global coordinate system. The transformation is loaded directly from the geometry constructed in the memory. We do not want to deal with true alignment here. The appropriate container node is found and its global transformation matrix is retrieved. Local coordinates of the hit are recalculated by ROOT matrix operations. This is done using a special singleton of so called GeoCache which stores useful information about sensor during geometry creation and contains also a transformation matrix from global volume to local coordinate system. However, this requires the geometry to be already built in the memory. For running the analysis module, the geometry parameter loader (GearBox module) and the geometry builder module (Geometry module) has to be present in the execution path before the analysis module. This solution ensures that the misalignment parameters of the geometry can be read from the geometry. Inspection of the analysis has proved perfect correspondence of residuals' mean values with aligned and unaligned geometry with applied correction transformations.

[7] This is the same only if the normal distribution "fits" the data, of course. Consequently, all misalignment corrections have to be carried out before fit is calculated by ROOT.

After space points from all sensors are known, the analysis continues with additional loop over sensors and fills fit data. Exclusive fit parameters are calculated and exclusive residuals are obtained by subtraction of fit prediction values from hit coordinates. For every single hit, its coordinates, residuals, cluster charge and cluster size information (obtained from PXDClusters) is used to fill a data object (TBTrackHit) which is stored in the DataStore.

Final analysis of ROOT histograms (like fitting) is done in ROOT independently on the analysis module.

7. Results

In this chapter, results of the simulation and analysis of the beam test in basf2 are presented. First part covers the results for 2009 beam test setup plus an energy scan. It deals with effects simulated by the basf2 PXD digitizer and clusterizer, evaluates residuals and shows an example of cluster charge/size/seed analysis. Comparison with experimental results is also presented and discussed in the discussion. Finally, the basf2 digitizer is used to simulate thinned (75 μm) matrix with Belle II design (pitch of 50 μm). Next to the high energy beam test simulation, conditions similar to Belle II environment have been simulated within an angle scan and the residuals and cluster size dependencies are shown. Most results are summarized in Table 6 in the attachments together with comparison to available experimental data from the 2009 beam test.

7.1 ILC Matrix Results

Let's focus on the 2009 beam test simulation of the 450 μm thin ILC-type DEPFET matrices at the nominal pion momentum of 120 GeV/c. The contribution of the multiple scattering (MS) to residuals (and telescope system resolution) can be evaluated by fitting points produced by Geant4 simulation (SimHits) before the charge collection is done. Thus, the effect of the digitizer and clusterizer is completely absent. Results are in quite a good correspondence with values evaluated in [14]. Comparison can be found in Table 3, in the discussion, Figure 21, and in Table 6 (where residuals for all sensor planes can be found) in the attachments. With digitizer and clusterizer turned on, the charge collection and clustering algorithm emulate the response of a real DEPFET sensor.

	Residual U [μm]		Residual V [μm]		MS Residuals [μm]	
Sensor	Simulation	Exp.	Simulation	Exp.	Simulation	Exp.
DUT	**1,28**	1,42	**1,83**	1,54	**0,7**	0,76
TEL3	**1,51**	1,61	**3,32**	1,98	**0,72**	0,79

Table 3: Comparison of residuals evaluated in the simulation to experimental values from [14] for the ILC DUT (450 μm thick, 20 μm pitch) and a reference telescope. The column „MS Residuals" show the residuals evaluated before the digitization and clusterization. Error of all values are in range of 0.1 μm.

Figure 12 shows residuals at the position of the DUT and a reference sensor (telescope TEL3) in a dependence on the cluster size. Apparently, the *v*-residuals of TEL3, do not have a single Gaussian shape. Similar pattern can be found in all the telescopes, which have pitch of 24 x 32 μm^2. However in this telescope, this effect is most apparent, because contribution of multiple scattering and telescope system error is very small at the position of TEL3. For evaluation of the width of these distributions, the variance of a Gaussian fit is still used rather than RMS to somehow estimate the width of the residual distribution. As a result, the residuals in *v*-direction have systematically shifted values to higher residuals than observed in the experimental beam test. In Figure 12 (bottom row), you can see that the unusual residual distribution is connected with cluster with size of 2. That means, the clustering algorithm has been used to compute position of the hit. The main reason for this behavior is an absence of an η-correction in our analysis, which deals with nonlinearities of the DEPFET pixel. See the discussion for more information and comparison to the experimental beam test.

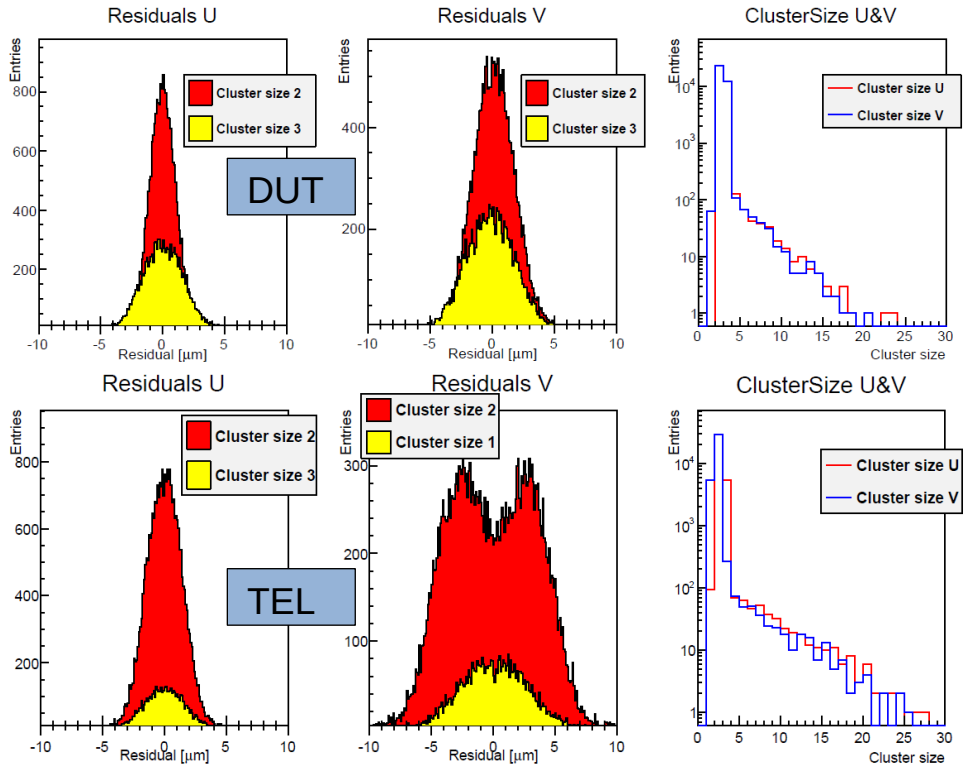

Figure 12: ILC pixel with thickness of 450 µm in the beam test simulation. 40k primary pions, momentum 120 GeV/c. Residuals in *u* and *v* directions for two most frequent cluster sizes for the DUT (top row) and TEL3 (bottom row). Cluster size in both directions is shown in logaritmic scale (last column).

For the 20 x 20 μm^2 DUT, the simulation (with charge collection and clustering) reproduces experimental values with satisfactory precision (even without the η-correction) and the residuals are Gaussians with longer tails, see Figure 13 and Figure 15 for visual comparison with beam test experimental results. Figure 13 also shows the distribution of cluster charge and seed charge for 120 GeV/c pions. Because the most frequent cluster size in the DUT is 2, the seed charge is visibly lower than the total cluster charge, because the charge is shared among more pixels. In Figure 14, you can find a typical total cluster charge distribution from the experimental beam test.

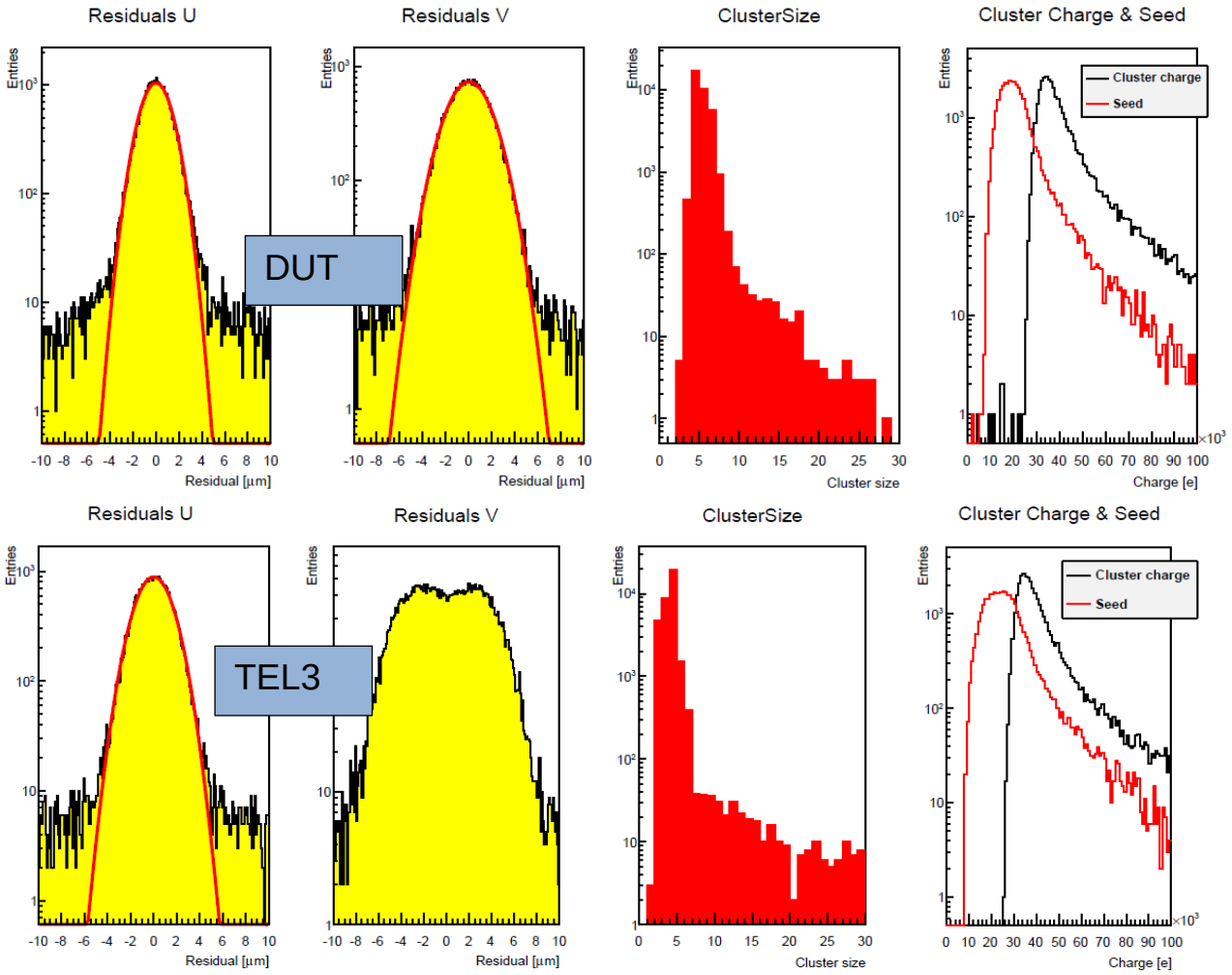

Figure 13: DUT 20 x 20 μm^2 pixel (top row) and TEL3 32 x 24 μm^2 (bottom row) in 2009 beam test simulation. Thickness of sensor is 450 µm. Simulation with 40k primary pions, 120 GeV/c. The Gaussian fit (red line) to residuals (for all cluster sizes) in logarithmic scale is shown; together with total cluster size I log scale. The cluster charge with seed charge in log scale (in red) distribution is on the right. Compare the cluster size to Figure 14. The cluster charge and seed distribution is in unit of elementary charge.

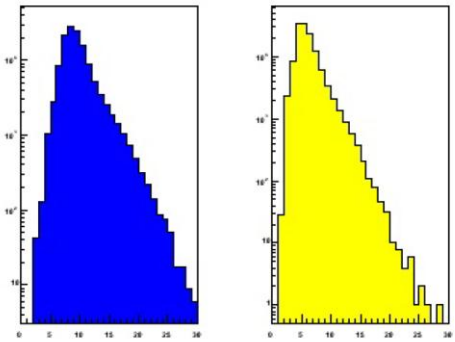

Figure 14: Typical cluster size distribution in logarithmic scale in the experimental beam test for DUT (left) and the reference telescope TEL3 (right). The horizontal axis has range of 30 units, same as in Figure 13. [14]

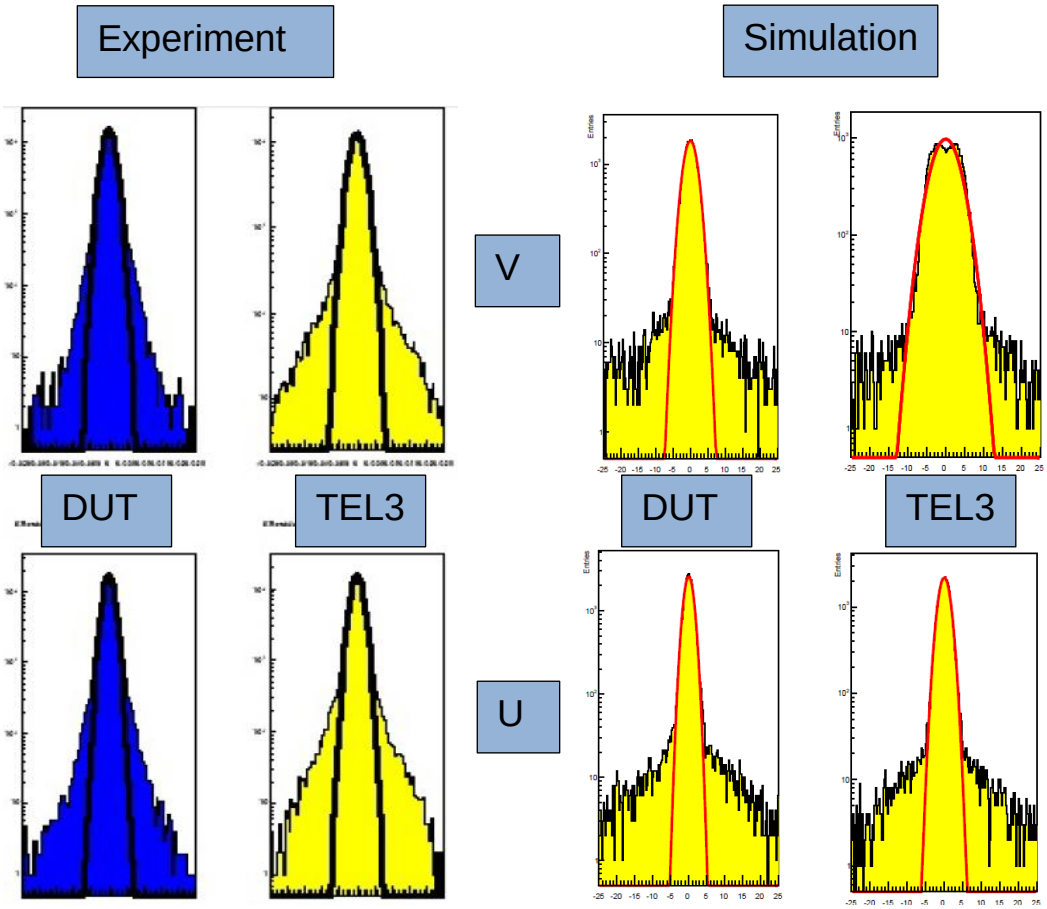

Figure 15: Comparison of simulation (right) and experimental (left) residual distributions in log scale for 40k primary pions, 120 GeV/c, in *v*-direction (top row) and *u*-direction (bottom row). Horizontal axes are in range of ±25 μm. [14]

A classical approach to evaluate detector resolutions is an energy scan and a plot of squared residuals versus squared inverse energy. *The result is a straight line with intercept equal to the sum of squared DUT resolution plus squared telescope*

system resolution in the DUT plane [15]. Although this thesis does not focus on the resolutions, these can be calculated from the energy scan, see Figure 16 (which shows also infinite energy extrapolation) and Table 6 in the attachments for numerical values. It should be noted, that the telescope system resolution has to be subtracted from these extrapolations to get true resolutions. [15]

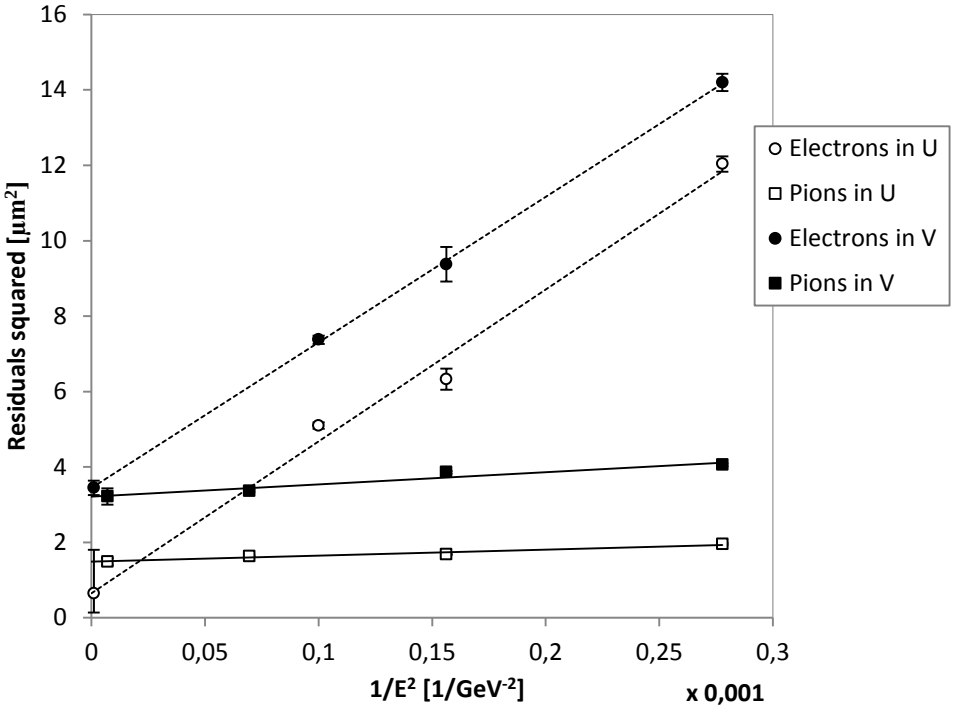

Figure 16: Simulation of the ILC DUT (450 µm thin, 20 µm pitch): Energy scan of squared residuals of ILC DUT in *u* and *v*-direction for pions (120, 80, 60 GeV/c) and electrons (100, 80, 60 Gev/c). Markers near zero (slightly shifted for better visibility) show predictions of the linear fit with errors. Fit results are shown in Table 4, values for the data points in this graph can be found in Table 6 in the attachments – for all sensor planes.

	Inf. energy extrapolation [µm]	
	u	v
Electrons	0.8 ± 0.7	1.86 ± 0.05
Pions	1.22 ± 0.04	1.79 ± 0.06

Table 4: Extrapolation of residuals to infinite energy for electrons and pions with the 20 x 20 μm^2 DUT.

Obviously, the fit fails to predict the extrapolation for electrons in *u*-direction with sufficient precision. One may expect the value for the electrons to be higher

than for pions at zero energy. For electrons, the bremsstrahlung plays an important role and typically causes worse stability of the residuals. Values for residuals for all sensors and each energy and particle in the energy scan are summarized in Table 6.

7.2 Belle II Matrix Results

The 120 GeV/c pion beam is used to probe the Belle II DEPFET matrix in the same telescope system as in the 2009 beam test. Residuals and cluster related quantities are showed in Figure 17 and in Table 6 in the attachments. This matrix has pitch of 50 μm in both directions. As a result, most clusters are only single pixel response – all charge goes to one pixel and the clustering algorithm is even not started. This can be seen also in the seed distribution, Figure 17, having nearly the same mean value as the charge distribution. Note the hump at lower charge which corresponds to clusters with response of more than one pixel – thus the charge is shared among more pixels – and the seed gets lower. Residuals with cluster size 1 are "box distributions" (see Figure 20 for 2D plot) – flat on the top. This is because hits from most of the pixel area end up with the same position in the middle of the pixel after digitization and the error of position estimation is $\mathrm{PITCH} \times \frac{1}{\sqrt{12}}$ (which gives 14,4 μm for 50 μm pitch). See Table 5 for overview of the residuals and Figure 18 for visual comparison to experimental distribution.

		Residuals [μm]		
Beam	Sensor	U	V	MS contr.
120GeV/c	DUT	14,66	14,61	0,55
Pions	TEL3	2,29	2,59	0,7
2 GeV/c	DUT	54	55	50
Electrons	TEL3	78	79	73

Table 5: Simulation residuals for Belle II type matrix (50 μm pitch, 75 μm thin) for high momentum pion beam (errors of residuals in range of 0.1 μm) and the 2 GeV/c electron beam (errors of residuals in range of 1 μm). The right – most column shows residuals of Geant4 SimHits before digitization.

Electron beam with momentum of 2 GeV/c has been used to make an angle scan with the Belle II matrix. The geometry is the same as for previous simulations. The DUT is rotated in the *xz* plane, see Figure 9. The straight line approximation is a bit worse in this case; since the residuals from multiple scattering at the position of the DUT go to ~ 50 μm and in the telescopes even to ~ 0.1 mm, see Table 5, or Table

6 in the attachments for detailed summary. Evaluated residuals at zero angle (tracks perpendicular to the sensor plane) can be found in Table 5 for overview and in Table 6 in the attachments for complete list of residuals at all sensor planes. Figure 19 shows the results of the angle scan – residuals and cluster sizes (with RMS as error bars) in both directions.

For visual comparison of the residuals for ILC and Belle II type DEPFET's in different simulation scenarios, see Figure 20, where 2D distributions of residuals are plotted. The "box distribution" for Belle II matrix for 120 GeV/c pions is clearly visible. At lower energies with electrons, the multiple scattering contributions exceed the residuals from digitization and the result is very wide Gaussian-like distribution with long tails. See Table 6 in the attachments for numerical values.

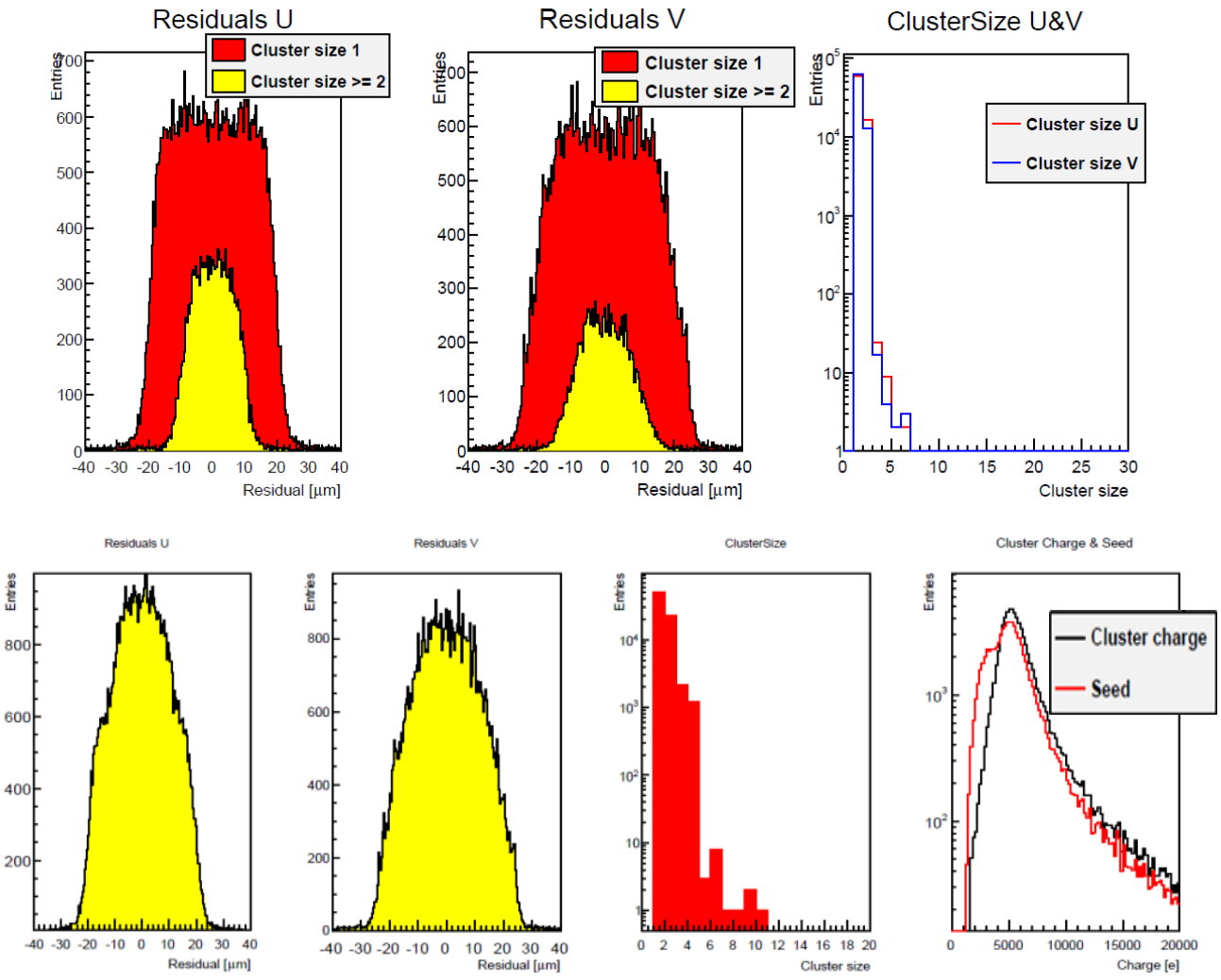

Figure 17: Simulation of Belle II 50x50 matrix with 120GeV/c pions, 80k primary particles. Top row shows distribution of residuals for the most frequent cluster sizes

and size of the clusters for both directions. Residuals for all cluster sizes are shown together with total cluster size in logarithmic scale and comparison of cluster charge and seed charge (bottom row) in log scale. The cluster charge and seed distribution is in units of elementary charge.

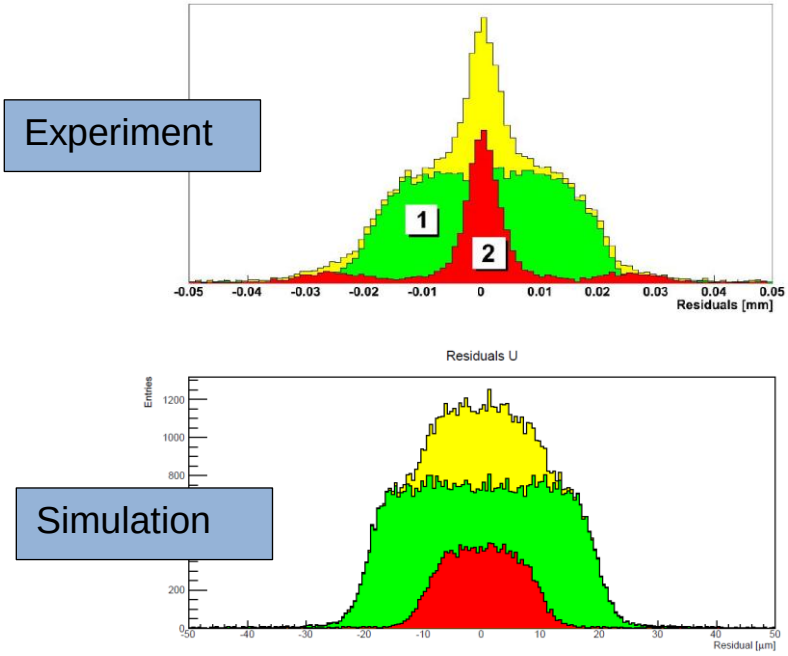

Figure 18: Comparison of residual distribution from the simulation (Belle II matrix with thickness of 75 µm) (bottom) and from first experimental results with 50 µm thin matrix with Belle II design (Pith of 50 µm). Residuals from single pixel response are shown in green, residuals from more than one pixel response (cluster size > 1) are shown in red. Total cluster size is in yellow. The range of both horizontal axis is the same: ±50 µm. *KODYŠ, P. The DEPFET Active Pixels for Belle II - Resolution in 50 micron Thinned Sensor.*

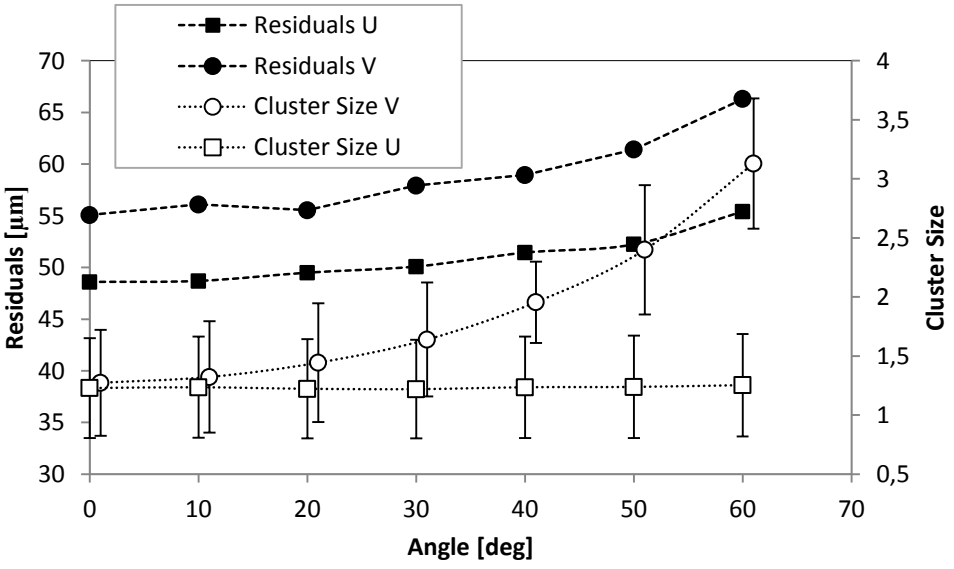

.

Figure 19: Angle scan with 2 GeV/c electrons for the Belle II DEPFET matrix with pitch of 50 µm. (20k primary particles, but efficiency is lower for nonzero angles)

Errors for residuals are approximately 1 µm. The error bars for cluster size show the RMS of the cluster size distribution to show the width of the distribution.

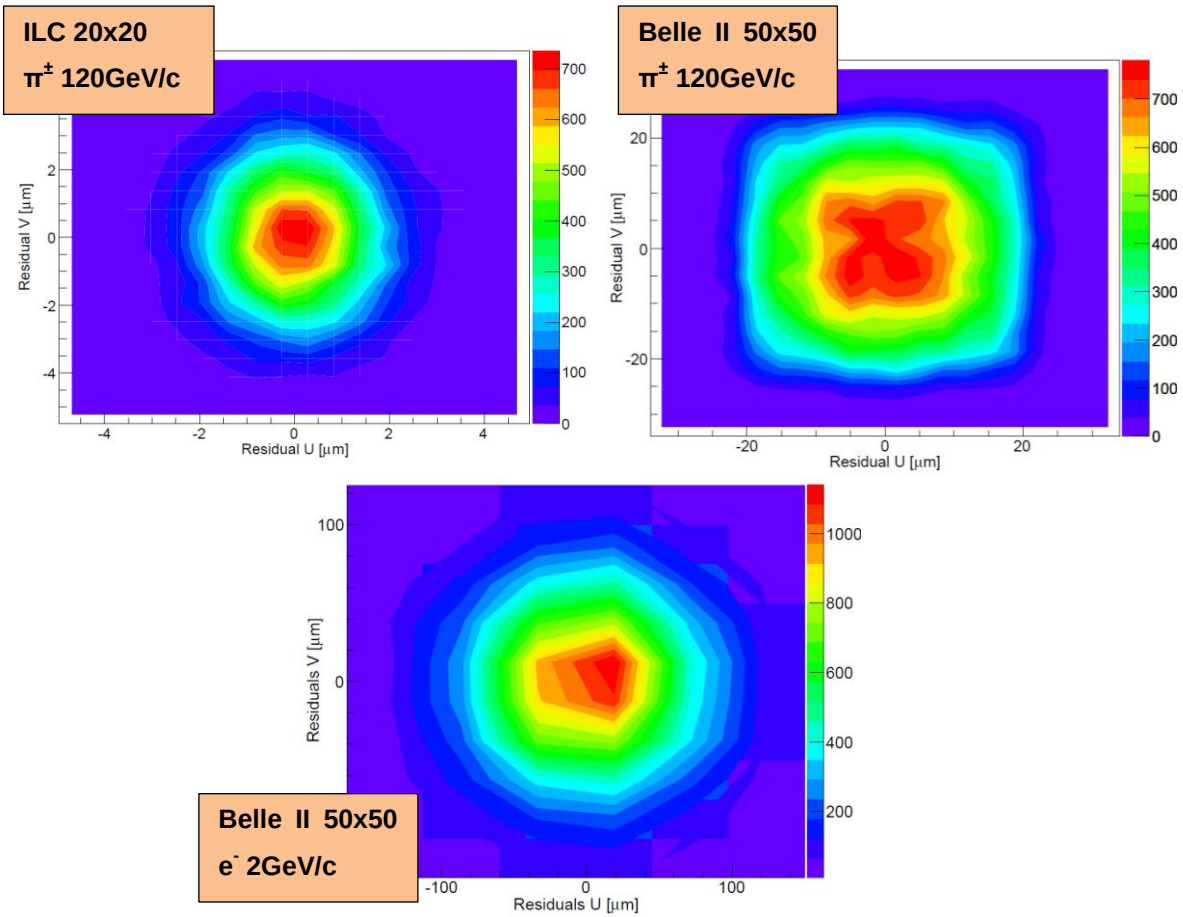

Figure 20: Simulation results: comparison of the spread of residual distributions in 2D histograms for different DUT‘s and simulation scenarios. The color axis shows number of entries (total number of hits is different). Note different scales of the histograms in the horizontal and vertical axis and the corresponding spread of the residuals.

8. Discussion

The beam test simulation in basf2 has been developed. It uses basf2 PXD digitizer and clusterizer to simulate detector response. The ILC-type pixels are simulated by setting appropriate configuration of the PXD modules, see section 4.1 and 5.3. Availability of experimental results for ILC-type pixels allows validation of the simulation results. The multiple scattering is reproduced with satisfactory precision, see Figure 21 (two bottom lines) for comparison to values extracted from the 2009 beam test at CERN.

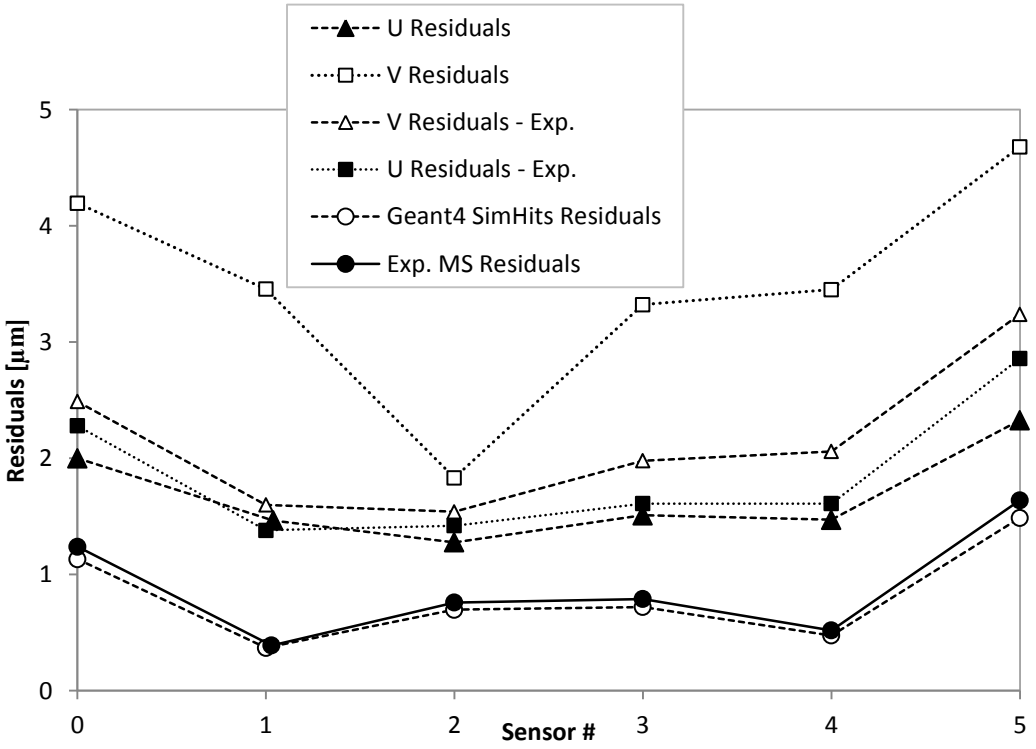

Figure 21: Comparison of experimental and simulated results for 120 GeV/c pions and ILC-type DUT. Errors of all points are in range of 0.1 µm.

The residuals after digitization and clustering are also compared to experimental data in Figure 21. While the residuals in *u*-direction are in quite a good agreement with experimental values, the *v*-direction resolutions are systematically worse than expected (difference almost 2 µm). The distributions of the residuals at telescope planes share a non-Gaussian pattern; see Figure 12 (bottom row).

Also, the cluster charge distribution shown in Figure 13 shows difference from experimental distribution shown in Figure 14. The reason for the "missing" cluster size is not accurate modeling of delta electrons. Especially in thin layer of

silicon, the delta electrons can significantly influence the cluster size and consequently the residuals. However, the production of the delta electrons cannot be changed in the basf2 framework at this development stage. It is known in the collaboration, that for realistic behavior, the range cut for delta electrons production in silicon should be adjusted to 10 μm (32 keV) for 450 μm thick matrix and to 4 μm (9 keV) for 75 μm thin Belle II sensor. The internal setting of basf2 is 20 μm for the range cut, which causes lower than realistic delta electron production.

There are two main reasons which together lead to deviations from expected residual distribution in the telescope. Next to the delta-electrons problem, the charge collection simulation is not optimal for telescopes' 24x32 pixels. Values in Table 2 are only estimations for the larger ILC pixel, the whole digitizing procedure is an approximation (even no lateral drift fields are simulated) and the wide narrow channel between regions with no charge collection simulation in Figure 11 influences charge sharing between pixels in the *v*-direction. The second and more important reason is absence of an η-correction in our analysis which deals with nonlinearities in the pixel. The η-variable (in one dimension) is defined as

$$\eta = \frac{S_{\mathrm{R}}}{S_{\mathrm{R}} + S_{\mathrm{L}}}, \tag{12}$$

where $S_{\mathrm{R(L)}}$ is the signal on the right (left) pixel in the cluster [18]. However, the model of charge collection used by the PXD digitizer uses large region with no charge collection. For perpendicular tracks, the spread of the charge in the readout plane depends mainly on the size of the diffusion cloud at the readout plane. If the cloud ends up entirely in the region with no charge collection, it is assigned to the respective internal gate inside, and S_{R} or S_{L} is zero ($\eta = 0$ or 1) because only one pixel gives signal. On the other hand, if the electron cloud gets a bit from this region, the charge sharing quickly grows and the clustering algorithm can be stared to predict hit position by the center of gravity algorithm. This results in nonlinearities in charge sharing and hit reconstruction and produces the "bad shape" of residuals with two symmetric peaks around zero (because evaluation of the residuals is based on assumption of linear charge sharing). [18]

For the small 20x20 ILC pixel, the diffusion cloud at the readout plane is wide enough to put some charge outside the internal gate region in almost all hits and

thus the charge sharing is closer to linear. The results for this pixel type are in good agreement with the experiment.

Results for the Belle II 50x50 matrix are also presented. This matrix has a pitch of 50 μm in both directions. Most clusters for perpendicular tracks are only single pixel response and the residuals have a form of "box distributions" (see Figure 20, top right corner, for 2D plot). This is because hits from most of the pixel area end up with the same position in the middle of the pixel after digitization (therefore the residual for a hit is equal to its distance from the center of the pixel in case of the single pixel response). Results for this matrix are also quickly compared to the simulation in Figure 18, where the most apparent difference is absence of small residual "hills" far from zero and wider peak for more than one cluster response. It should be noted, that the presented picture has not the same thickness (50 versus 75 μm) and delta electron production is not optimal. The dependency of the cluster size and the residuals on the incidence angle has been studied in the angle scan, see Figure 19.

Conclusion

The beam test setup has been completely implemented in basf2. Finally, cooperation of all components in the framework has been established. Results of the simulations have been thoroughly studied to truly understand software behavior, mostly because many parts of the basf2 framework are still under development. A new DEPFET digitizing module has been developed in the collaboration during work on this thesis and used in the simulation. The developed simulation allows studying different beam test geometries and the behavior of the digitizer and clusterizer in basf2.

The multiple scattering contributions have been successfully reproduced in the simulation. The results of digitization are in good agreement with experimental values for the small ILC DEPFET matrix used for the DUT. Larger ILC DEPFET matrices in telescopes give wrong results in the v-direction, which could be corrected by introducing the η-correction in the analysis; see the discussion for more details.

Finally, the beam test simulation has been used to simulate Belle II DEPFET matrix. It is important to note, that the simulation used exactly the same PXD digitizer, which is used in basf2 to simulate the Belle II PXD sub-detector. Default basf2 settings for all values have been used to study the DEPFET detector in high energy conditions and at lower energies within an angle scan.

The developed simulation can be upgraded by additional modules performing further analysis, tracking or loading external data for analysis. It is going to become a part of the official basf2 release and to simulate further PXD beam tests directly in the basf2 environment.

Results of this thesis and subsequent basf2 development have been presented at the 4th Belle II Computing Workshop in Ljubljana, Slovenia, and the 5th Belle II Computing Workshop at KEK, Japan.

Bibliography

[1] The Nobel Foundation. *The Nobel Prize in Physics 2008. Nobelprize.org* [online]. Last update 22 May 2012 [cit. 12/05/22]. <http://www.nobelprize.org/nobel_prizes/physics/laureates/2008/>

[2] DOLEŽAL, Zdeněk. Super KEKB and Belle II: Status of the KEK Super B Factory. arXiv:0910.0388v1 [hep-ex]. 2 Oct 2009.

[3] University of California. *Particle Data Group* [online]. c2012 [cit. 12/05/22]. <http://pdg.lbl.gov>

[4] ŽÁČEK, Josef. *Úvod do fyziky elementárních částic*. Praha: Karolium, 2005. ISBN 80-246-1109-0

[5] Z. DOLEŽAL, S. UNO et al. Belle II Technical Design Report. arXiv:1011.0352v1 [physics.ins-det], 1 Nov 2010

[6] HARA, Takanori. *Belle II Web Page* [online]. Last update 2012/05/17 [cit. 2012/05/22]. <http://belle2.kek.jp>

[7] High Energy Accelerator Research Organization, KEK. *New electronics tested for Belle II central drift chamber* [online]. Last update 2010/03/23 [cit. 2012/05/22]. <http://www.kek.jp/intra-e/feature/2010/BelleIICDCDesign.html>

[8] DRÁSAL, Zbyněk. Simulation of Charge Collection in Semiconductor Microstrip Detectors. Prague, 2006. Diploma thesis, Charles University in Prague, Faculty of Physics and Mathematics. Supervisor of the diploma thesis: Zdeněk Doležal.

[9] Max-Planck-Institut für extraterrestrische Physik and Max-Planck-Institut für Physik. *Research Activities* [online]. München: MPI Halbleiterlabor, Juni 2007 [cit. 2012/05/22]. <http://www.hll.mpg.de/graphics/MPI-HLL-brochure07b.pdf>

[10] HARA, Takanori, et al. *The basf2 Framework, an introduction* [online]. 16/06/2010 [cit. 2012/05/22]. <http://indico.ifj.edu.pl/MaKaC/getFile.py/access?contribId=1&sessionId=1&resId=0&materialId=slides&confId=22>

.[11] BRUN, R. et al. *ROOT | A Data Analysis Framework* [online]. c2012 [cit. 2012/05/22]. <http://root.cern.ch>

[12] GEANT4 Collaboration. *Geant4: A toolkit for the simulation of the passage of particles through matter* [online]. Last update 2012/05/16 [cit. 2012/05/22]. <http://www.geant4.org>

[13] HARA, Takanori – KUHR, Thomas. *Basf2 Software Portal* [online, password protected]. Last revision 2012/04/19 [cit. 12/05/22]. <http://ekpbelle2.physik.uni-karlsruhe.de/~twiki/bin/view/Computing/>

[14] KODYŠ, P. et al. *DEPFET Beam Test 2009 - Prague Analysis Report. Internal DEPFET note* [online]. July 2010 [cit. 12/05/22] <http://aldebaran.hll.mpg.de/twiki/pub/DepfetInternal/TBResults2009PraguePage/201004_TB2009PrgAnal_Rel2.pdf>

[15] L. ANDRICEK, J. CARIDE, Z. DOLEŽAL et al. Intrinsic resolutions of DEPFET detector prototypes measured at beam tests. *Nuclear Instruments and Methods in Physics Research*, Volume 638, Issue 1, 11 May 2011, Pages 24-32, ISSN 0168-9002.

[16] Private correspondence with Benjamin Schwenker, Universität Gottingen.

[17] KVASNIČKA, P. et al. *DEPFET Beam Test Alignment and Detector Resolution Analysis. Internal DEPFET note* [online]. Prague, August 2007 [cit. 12/05/22]. <http://aldebaran.hll.mpg.de/twiki/bin/viewfile/DepfetInternal/TBAnalysisPraguePage?rev=1;filename=DEPFET_TB_Alignment.pdf>

[18] TURCHETTA, R., *Nuclear Instruments and Methods in Physics Research* A 335 (1993), Pages 44–58.

[19] ENGLICH, J. Zpracování výsledků fyzikálních měření [online]. Prague, 2000 [cit. 12/05/22]. <http://physics.mff.cuni.cz/vyuka/zfp/mereni.pdf>

Attachments

1) Software

On the attached CD-ROM, one can find the source code of the beam test simulation. For running the software, one needs to have basf2 framework installed. The `testbeam/` directory on the CD-ROM must be placed into the `pxd/` directory located under basf2 `release/` directory.

Unfortunately, basf2 is not publicly available. To get an access to the basf2 Software Portal [13], it is necessary to obtain a password from the Belle II Collaboration. On the basf2 Software Portal, the installation process of the basf2 framework is described with links to its source code and access to subversion repository (https://ekpbelle2.physik.uni-karlsruhe.de/trunk/software). After basf2 installation (you need to install at least these packages: framework, geometry, generators, pxd, vxd, simulation), the beam test can be copied to the PXD package directory. Finally the basf2 compilation must be run once again.

The included version of the beam test simulation works in the basf2 subversion **revision 2778** (Changed Date: 2012/03/18). Because basf2 is still under development and some features may change, it is highly recommended to use only this revision of basf2 for the beam test source code included on the CD-ROM.

Example steering scripts are included in the `testbeam/steering/` directory. The whole source code contains a number of comments, including description of the parameters in the steering scripts. Included `ReadMe.txt` file contains additional instructions.

The source code (with updates) can be also found online at:

http://www-ucjf.troja.mff.cuni.cz/kodys/works/uceni/en/Bilka_Basf2_testbeam.zip

2) Table with summary of results

The attached Table 6 contains results of residual evaluation for studied simulation scenarios and provides also the experimental data for comparison, where available. It summarizes the energy scan and contains complete list of residuals at all sensor planes for the simulation of the ILC and Belle II type DEPFET matrices.

		Residuals [μm]							
		Sensor #	SimHits U	SimHits V	Exp. MS	Digitized U	Exp. U	Digitized V	Exp. V
Electrons 60 GeV/c	ILC type matrix. Pitch [μmxμm]: 24 x 32 for sensor # 0, 1, 3, 4, 5 | 20 x 20 for sensor # 2 (DUT)	0 (TEL1)	5.27	5.27	-	5.69	6.67	7.23	6.87
		1 (TEL2)	1.56	1.56	-	2.31	4.31	4.10	4.41
		2 (DUT)	**3.06**	**3.04**	**-**	**3.47**	**5.25**	**3.77**	**5.35**
		3 (TEL3)	3.25	3.27	-	3.67	5.52	5.02	5.58
		4 (TEL4)	1.96	1.96	-	2.56	4.80	4.32	5.08
		5 (TEL5)	6.53	6.54	-	6.85	7.97	8.69	8.71
Electrons 80 GeV/c		0 (TEL1)	3.57	3.43	-	4.26	4.73	6.17	5.06
		1 (TEL2)	1.06	1.09	-	1.90	3.12	3.92	3.40
		2 (DUT)	**2.05**	**2.01**	**-**	**2.52**	**3.85**	**3.06**	**3.84**
		3 (TEL3)	2.08	2.05	-	2.94	3.98	4.36	4.23
		4 (TEL4)	1.35	1.37	-	2.11	3.62	4.02	3.80
		5 (TEL5)	3.93	4.84	-	5.49	5.49	7.04	6.08
Electrons 100 GeV/c		0 (TEL1)	2.76	2.79	-	3.85	4.03	5.53	4.10
		1 (TEL2)	0.91	0.91	-	1.83	2.40	3.71	2.73
		2 (DUT)	**1.75**	**1.75**	**-**	**2.26**	**3.04**	**2.72**	**3.28**
		3 (TEL3)	1.85	1.83	-	2.58	3.38	4.14	3.56
		4 (TEL4)	1.16	1.16	-	1.99	2.92	3.86	3.49
		5 (TEL5)	3.40	3.56	-	4.94	4.51	6.51	4.75
Pions 60 GeV/c		0 (TEL1)	2.22	2.19	-	2.56	-	5.05	-
		1 (TEL2)	0.69	0.70	-	1.27	-	4.73	-
		2 (DUT)	**1.37**	**1.36**	**-**	**1.96**	**-**	**4.06**	**-**
		3 (TEL3)	1.42	1.42	-	2.19	-	3.70	-
		4 (TEL4)	0.92	0.93	-	1.99	-	3.80	-
		5 (TEL5)	2.87	2.90	-	3.59	-	6.45	-
Pions 80 GeV/c		0 (TEL1)	1.67	1.66	-	2.06	2.83	4.77	3.05
		1 (TEL2)	0.52	0.52	-	1.18	1.48	4.67	1.73
		2 (DUT)	**1.03**	**1.03**	**-**	**1.68**	**1.75**	**3.86**	**1.86**
		3 (TEL3)	1.06	1.05	-	1.96	1.90	3.58	2.26
		4 (TEL4)	0.69	0.69	-	1.90	1.76	3.71	2.19
		5 (TEL5)	2.19	2.16	-	2.94	3.55	6.14	3.78
Pions 120 GeV/c		0 (TEL1)	1.13	1.13	1.24	2.00	2.28	4.20	2.49
		1 (TEL2)	0.37	0.37	0.39	1.46	1.38	3.46	1.60
		2 (DUT)	**0.70**	**0.70**	**0.76**	**1.28**	**1.42**	**1.83**	**1.54**
		3 (TEL3)	0.72	0.73	0.79	1.51	1.61	3.32	1.98
		4 (TEL4)	0.48	0.48	0.52	1.47	1.61	3.45	2.06
		5 (TEL5)	1.49	1.50	1.64	2.33	2.86	4.68	3.24
	Belle II matrix 50 x 50 μm^2 as DUT	0 (TEL1)	1.01	1.01	-	5.17	-	5.64	-
		1 (TEL2)	0.37	0.37	-	3.50	-	3.88	-
		2 (DUT)	**0.55**	**0.55**	**-**	**14.66**	**-**	**14.61**	**-**
		3 (TEL3)	0.70	0.70	-	2.29	-	2.59	-
		4 (TEL4)	0.48	0.48	-	2.09	-	2.37	-
		5 (TEL5)	1.42	1.42	-	2.80	-	3.08	-
Electrons 2 GeV/c		0 (TEL1)	102	93	-	106	-	107	-
		1 (TEL2)	42	40	-	42	-	42	-
		2 (DUT)	**51**	**49**	**-**	**54**	**-**	**55**	**-**
		3 (TEL3)	77	69	-	78	-	79	-
		4 (TEL4)	55	50	-	54	-	55	-
		5 (TEL5)	142	134	-	142	-	143	-

Table 6: Summary of residuals of the Geant4 SimHits (without digitization and clustering) and residuals after detector response simulation (the "Digitized" columns) for different simulation scenarios. Values are compared to the experimental beam test data from [14] where available (See the "Exp." columns). Errors are in range of 0.1 μm except the last 6 rows, where residual errors are in range of micrometers.